



Contents lists available at ScienceDirect

Science of the Total Environment

journal homepage: www.elsevier.com/locate/scitotenv

16S rRNA metabarcoding unearths responses of rare gut microbiome of fathead minnows exposed to benzo[*a*]pyrene

Abigail DeBofsky^a, Yuwei Xie^{a,*}, Jonathan K. Challis^a, Phillip J. Ankley^a, Markus Brinkmann^{a,c}, Paul D. Jones^{a,c}, John P. Giesy^{a,b,d}

^a Toxicology Centre, University of Saskatchewan, Saskatoon, Saskatchewan, Canada

^b Department of Veterinary Biomedical Sciences and Toxicology Centre, University of Saskatchewan, Saskatoon, Saskatchewan, Canada

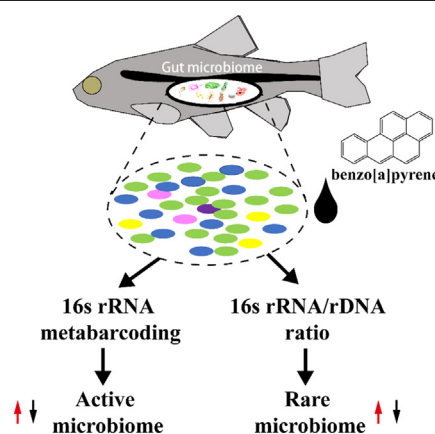
^c School of Environment and Sustainability, University of Saskatchewan, Saskatoon, Saskatchewan, Canada

^d Department of Environmental Science, Baylor University, Waco, TX, USA

HIGHLIGHTS

- Active gut microbiome was significantly different from the genomic gut microbiome.
- Dietary BaP exposure altered active gut microbiomes of juvenile fathead minnows.
- rDNA-normalized revealed hidden responding patterns of rare taxa to BaP exposure.

GRAPHICAL ABSTRACT



ARTICLE INFO

Article history:

Received 26 June 2021

Received in revised form 23 September 2021

Accepted 14 October 2021

Available online xxx

Editor: Jay Gan

Keywords:

Homeostasis

Next-generation sequencing

Freshwater fish

Persistence organics pollution

Molecular ecology

16S metagenomics

ABSTRACT

Activities of gut microbiomes are often overlooked in assessments of ecotoxicological effects of environmental contaminants. Effects of the polycyclic aromatic hydrocarbon, benzo[*a*]pyrene (BaP) on active gut microbiomes of juvenile fathead minnows (*Pimephales promelas*) were investigated. Fish were exposed for two weeks, to concentrations of 0, 1, 10, 100, or 1000 $\mu\text{g BaP g}^{-1}$ in the diet. The active gut microbiome was characterized using 16S rRNA metabarcoding to determine its response to dietary exposure of BaP. BaP reduced alpha-diversity at the greatest exposure concentrations. Additionally, exposure to BaP altered community composition of active microbiome and resulted in differential proportion of taxa associated with hydrocarbon degradation and fish health. Neighborhood selection networks of active microbiomes were not reduced with greater concentrations of BaP, which suggests ecological resistance and/or resilience of gut microbiota. The active gut microbiome had a similar overall biodiversity as that of the genomic gut microbiota, but had a distinct composition from that of the 16S rDNA profile. Responses of alpha- and beta-diversities of the active microbiome to BaP exposure were consistent with that of genomic microbiomes. Normalized activity of microbiome via the ratio of rRNA to rDNA abundance revealed rare taxa that became active or dormant due to exposure to BaP. These differences highlight the need to assess both 16S rDNA and rRNA metabarcoding to fully derive bacterial compositional changes resulting from exposure to contaminants.

© 2021 Elsevier B.V. All rights reserved.

* Corresponding author at: Toxicology Centre, University of Saskatchewan, Saskatoon S7N 5B3, Saskatchewan, Canada.
E-mail address: yuwei.xie@usask.ca (Y. Xie).

1. Introduction

Like other vertebrates, fishes benefit from having host associated symbiotic gut microbiota. The gut microbiota contribute to the health of fish via important biological processes, including nutritional provisioning (Dimitroglou et al., 2011), regulation of intestinal barrier functions (Pérez et al., 2010), and immune defence (Egerton et al., 2018; Rolig et al., 2015). Facing environmental fluctuations, biodiversity of the gut microbiome is vital to stabilization of the internal ecosystem for proper functioning and host well-being (Van den Abbeele et al., 2013; Vinebrooke et al., 2004). Additionally, environmental contaminants can alter community structure resulting in disturbed homeostasis (Adamovsky et al., 2018; Claus et al., 2016), which is associated with several harmful outcomes, including chronic inflammation, metabolic syndromes, stress, and disease susceptibility (Carding et al., 2015; He et al., 2019; Kotas and Medzhitov, 2015; Llewellyn et al., 2014). A few approaches have been developed to study interactions between mammal gut bacteria and chemical pollutants, including cultured bacteria, fecal/gut microbiota suspensions, germ-free or antibiotic-treated animals, microfluidic intestines-on-chips, 3D bioengineered gastrointestinal models, and animals treated with microbiotas altered by environmental chemicals (Claus et al., 2016; Fois et al., 2019). However, due to limited knowledge of fish gut microbiota and fewer isolated bacteria from fish, these methods require additional refinement before being applied to fishes. Furthermore, most studies of fish microbiome have focused solely on the genomic composition of gut microbiome by use of 16S rDNA metabarcoding or metagenomics, which mainly targets both active and inactive abundant microorganisms (Egerton et al., 2018; Givens et al., 2015). This approach underestimates the active fraction of the gut microbiome, which is contributing to the actual metabolic functions in the gut.

Like other ecosystems, rare species of gut microbial ecosystems can play important roles in maintaining ecological homeostasis of gut microbiota and benefits to host fitness (Chen et al., 2016; Sfanos et al., 2018) via modulating hormone metabolites (Antwis et al., 2019) or the immune system (Rolig et al., 2015). Rare species provide disproportionately large functional contributions to species assemblages; however, they are vulnerable to anthropogenic disturbances (Leitão et al., 2016). It's still challenging to detect responses of rare species exposed to stressors because vertebrate gut microbiomes are typically dominated by a few abundant species and several less-abundant species (Jousset et al., 2017; Rolig et al., 2015). Experimental approaches, such as creating synthetic communities and manipulating natural communities, are useful to study rare species in environmental communities, but are hardly feasible for manipulating gut microbiota (Jousset et al., 2017). 16S rDNA and rRNA metabarcoding are powerful tools for characterizing rare microbiota, with 16S rRNA metabarcoding providing insight into the activity of the microbiome (Campbell et al., 2011; Jousset et al., 2017; Zhou et al., 2021). Compared to 16S rDNA metabarcoding, 16S rRNA metabarcoding serves as a potential proxy for protein-synthetic activity of the microbial community (De Vrieze et al., 2016), which can give information on low abundance taxa with high activity (Abu-Ali et al., 2018; Revetta et al., 2011). Integrated rDNA and rRNA metabarcoding can provide a comprehensive view for assessing responses of gut microbiome to chemical pollutants.

Understanding effects of chemical pollutants on fish gut microbial communities is complex because of the triad relationship between host physiology, gut microbiota, and chemical pollutants. Benzo[a]pyrene (BaP) is an ideal compound of persistent organic pollutants (POPs) to stimulate rare species of gut microbiota. BaP is the most well-studied polycyclic aromatic hydrocarbon (PAH), known to induce or promote tumor formation, as well as suppressing immune function (Beyer et al., 2010; Carlson et al., 2004a; Tuvikene, 1995). Additionally, BaP has well-characterized deleterious effects in fishes (Carlson et al., 2004b; Costa et al., 2011; Nacci et al., 2002; Phalen et al., 2014). BaP can alter fish gut microbiota, with increasing presence of hydrocarbon-degrading bacteria at low dosages (DeBofsky et al., 2020,

2021), and inflammation in the intestinal tracts at a high dose (Xie et al., 2020). The hydrocarbon-degrading bacteria are ubiquitous but rare in the environment (Xu et al., 2018), and their rareness in the gut microbiota of wild aquatic organisms is related to the level of habitat contamination (Šyvokiene and Mickeniene, 2011). Additionally, there are still knowledge gaps of the effects of BaP on active gut microbiomes of fish.

In order to investigate the response of the active microbiome, particularly that of rare microbiota, this study utilized dietary exposure of juvenile fathead minnows (*Pimephales promelas*) to a model compound, BaP. Dietary exposure is more effective to distribute BaP into gut-intestine track because it results in accumulation of BaP in the bile and intestine (Sandvik et al., 1998). Specific objectives were to: 1) Describe the active gut microbiome in juvenile fathead minnows; 2) Characterize the responses of the active gut microbiome to exposure of BaP; and 3) Compare responses of abundant and rare bacteria in gut to exposure of BaP. To satisfy these objectives, the active microbiome in guts of fathead minnows were characterized using 16S rRNA metabarcoding after dietary exposure to BaP for two weeks.

2. Materials and methods

2.1. Fish husbandry, dietary exposure, and sampling

Fish husbandry procedures have been fully described previously (DeBofsky et al., 2021). Briefly, laboratory-reared juvenile fathead minnows were acclimated at 25 ± 1 °C with a 16 h-light:8 h-dark photoperiod. Fish were fed EWOS® Micro Crumble trout chow (Cargill Inc., Wayzata, MN), twice daily on a maintenance food ration (2% of mean, wet body mass per day). After a one-week acclimation, fish were randomly assigned to each group ($n = 30$ per group; 3 tanks per group; 10 fish per tank), and exposed to a solvent control (0.02% methanol), or nominal concentrations of 1, 10, 100 or 1000 $\mu\text{g g}^{-1}$ dry mass (dm) of BaP in food for two weeks. Nominal concentrations were based on environmentally-relevant concentrations of PAHs found in highly contaminated sites (Claisse, 1989; Knutzen and Sortland, 1982). At the end of the exposure, fish were euthanized via cervical dislocation. The whole intestinal tract was excised from each fish to collect the microbiome, and gallbladders were removed for quantifying BaP metabolites. Thirty-two fishes were discarded due to sexual differentiation over the course of the exposure. Samples were stored at -80 °C before RNA extraction. All fish procedures followed the animal use protocol (#20090108) approved by the Animal Research Ethics Board at the University of Saskatchewan.

2.2. Quantification of BaP in food and BaP metabolites in bile

Detailed procedures of quantification of BaP in food and BaP metabolites in bile are available in DeBofsky et al., 2021. Briefly, internal calibration based on isotope dilution was used to quantify BaP in samples using an eight-point calibration curve between 0.5 and 500 ng mL^{-1} , each spiked at 100 ng mL^{-1} with BaP-d12. Triplicate 0.05 g aliquots of prepared food were spiked with BaP-d12 at a target concentration of 100 ng mL^{-1} in the final 1 mL extract. Each sample was extracted using an accelerated solvent extraction cell. Concentrations of monohydroxylated BaP (OH-BaP) were quantified directly by use of analytical standards and external calibration. Semi-quantification of OH-BaP-O-glucuronide (BaP-Gluc) and sulfate-BaP (BaP-SO₄) was accomplished by use of a relative response factor approach. Analysis was done by GC-QE-Orbitrap mass spectrometer system (Q Exactive, Thermo Scientific). Detailed results of the BaP in food and BaP metabolites in bile have been reported previously (DeBofsky et al., 2021). Nominal concentrations were confirmed by measuring concentrations of BaP in food (SI Table S1).

2.3. Metabarcoding and bioinformatics

The active gut microbiome was characterized by 16S rRNA metabarcoding. Total RNA was co-isolated with DNA from intestines

using the AllPrep DNA/RNA Mini Kit (Qiagen Inc., Mississauga, ON). Residual DNA was removed by on-column digestion with DNase I and ezDNase. Complementary DNA was synthesized with the SuperScript™ IV Reverse Transcriptase kit (ThermoFisher Scientific, Waltham, MA). PCR amplification of the V3-V4 region of the 16S rRNA gene, construction of the sequencing libraries and next-generation sequencing were performed as previously described (DeBofsky et al., 2021).

Sequences of 16S rDNA and rRNA metabarcoding were pooled and analyzed together in the same bioinformatics pipeline to compare rRNA active gut microbiome with rDNA-based genomic gut microbiome (DeBofsky et al., 2021). On average, 69% of demultiplexed reads survived through the cleaning process, and 99% of the cleaned reads could be aligned to bacteria. Numbers of reads per sample pre- and post-cleaning are summarized in SI Table S2. The feature table was rarefied at 13,133 sequences per sample to avoid biases introduced by different sequencing depths (SI Fig. S1). Thirty-four samples were removed due to low sequencing depth. Alpha- (Shannon diversity and number of observed amplicon sequence variants (ASVs)) and beta-diversities (Bray-Curtis dissimilarities) were calculated in QIIME2 (Bolyen et al., 2019). PICRUST2 (Douglas et al., 2019) was used to predict functional abundances of MetaCyc pathways (Caspi et al., 2017) based on 16S rRNA gene sequences. Data can be accessed at: <https://doi.org/10.20383/101.0247>.

2.4. Statistics

Statistical analyses were performed using R Statistical Language v. 3.6.1 (R Core Team, 2013). Assumptions of normality and equal variance were assessed, then depending on if assumptions of parametric statistics were met, either an analysis of variance (ANOVA) followed by a Dunnett's test, or a Kruskal Wallis followed by Mann-Whitney *U* test to compare exposure groups to the solvent control was used. Unless otherwise noted, statistics were completed using the 'vegan' package (Oksanen et al., 2019). Concentrations of predominant metabolites of BaP were log₁₀-transformed prior to statistical analysis. To avoid taking logs of zero, an arbitrary value of 0.0001 ng g⁻¹ was assigned to values below the detection limit. To retain as much microbiome data as possible, samples where the gall bladder was empty were assigned as the average value from their corresponding exposure group. Abundant ASVs/taxa were defined as those that comprise ≥1% of the community, and rare ASVs were <1%. The ratio of active gut microbiome to genomic gut microbiome was assessed independently to evaluate normalized activity of bacterial genus. The normalized activity was calculated (Eq. (1)).

$$\lambda_{f,i} = \frac{R_{f,i}}{\sum_f R_{f,i}} \div \left[\frac{D_{f,i}}{\sum_f D_{f,i}} + \frac{1}{2} \times \frac{t}{\sum_f D_{f,i}} \right] \quad (1)$$

$R_{f,i}$ and $D_{f,i}$ are the counts of feature/taxa f in sample i , for the rRNA metabarcoding and rDNA metabarcoding respectively. The variable t is the detection limit, here set to 1 read, and n is the sample size after filtering.

Differentially abundant bacterial taxa and MetaCyc pathways were calculated using the ANOVA-Like Differential Expression tool (ALDEx2) (Fernandes et al., 2013). Spearman correlations between taxa or MetaCyc pathways and log-transformed BaP-SO₄ (IgBaP-SO₄) were also computed by use of Aitchison's centered log-ratio (CLR)-transformed data. To determine differences among community composition based on nucleotide and exposure conditions, Bray-Curtis dissimilarities for log-transformed ASV values at the level of genera for each exposure group were assessed using 'adonis2' (Oksanen et al., 2019), and the pairwise.adonis2 function with Bonferroni p -value adjustment (Martinez Arbizu, 2019). A Constrained Analysis of Principal Coordinates (CAP) was conducted to ordinate the data and view the clusters

of samples as constrained by the log-transformed BaP metabolite data. Significant BaP metabolites contributing to the ordination were assessed using an ANOVA of the terms. To visualize community differences, bootstrapped Bray-Curtis dissimilarity averages of the genus tables for each exposure group were plotted using metric MDS (PRIMER-e v.7). Neighborhood selection network (Meinshausen and Bühlmann, 2006) was constructed by the SPIEC-EASI package (Kurtz et al., 2015).

3. Results

3.1. Active gut microbiome of juvenile fathead minnows

The active gut microbiome, as determined through 16S rRNA analysis, was diverse, but dominated by limited numbers of key bacterial taxa. In total, 1575 non-singletons active ASVs of 75 bacterial genera among 84 samples (n = control: 19, 1 μg g⁻¹: 15, 10 μg g⁻¹: 20, 100 μg g⁻¹: 15, 1000 μg g⁻¹: 15) were recovered using rRNA metabarcoding. The active gut microbiomes were dominated by (mean ± standard error) *Proteobacteria* (48% ± 1%), *Fusobacteria* (43.5% ± 1%), and *Bacteroidetes* (4% ± 0.4%) at the phylum level (Fig. S2A). The dominant classes were *Gammaproteobacteria* (46% ± 1%), *Fusobacteriia* (43% ± 1%), and *Bacteroidia* (4% ± 0.4%) (Fig. S2B). The dominant families were *Fusobacteriaceae* (43% ± 1%), *Aeromonadaceae* (26% ± 1%), and *Pseudomonadaceae* (13% ± 1%) (Fig. S2C).

rRNA metabarcoding detected more ASVs than rDNA metabarcoding (Welch's *t*-test: $t = -4.6$, $p < 0.001$). Fifty-eight genera were detected by both rDNA and rRNA metabarcoding, while six were unique to rDNA metabarcoding and 17 were unique to rRNA metabarcoding (Fig. S3A). The profile of the active gut microbiome was significantly different from that of the genomic gut microbiome (adonis test, $F = 5.5$, $p < 0.001$, Fig. S3B).

3.2. Dietary exposure of BaP altered active gut microbiome

Alpha-diversity of the active gut microbiome was less in groups that were exposed to BaP. Dietary exposure to BaP resulted in lesser Shannon diversity of the active gut microbiome (KW test, $\chi^2 = 12.9$, $p = 0.01$), which approached significance in the greatest exposure (1000 μg g⁻¹) group relative to the control group (Fig. 1). The fewer observed active ASVs based on exposure to BaP approached significance (ANOVA test, $F = 2.2$, $p = 0.08$), and the greatest exposure concentration (1000 μg g⁻¹) had significantly fewer ASVs than the control group (Fig. 1).

There was a significant effect of dietary exposure to BaP on community structure agglomerated to genus level (adonis test, $F = 3.2$, $p = 0.001$; Fig. 2A). The structure of the active gut microbiome was significantly affected by exposure to BaP at the greater exposure concentrations; while the control group community structure was not significantly different from the 1 or 10 μg g⁻¹ groups, it was significantly different from the 100 (Pairwise adonis test, $F = 2.4$, $p = 0.02$) and 1000 μg g⁻¹ (Pairwise adonis test, $F = 4.9$, $p = 0.001$) groups. Metabolites of BaP (log₁₀ transformed) significantly constrained the ordination of the CAP1 and CAP2 (ANOVA test, $p = 0.001$ and $p = 0.04$ for IgBaP-OH and IgBaP-SO₄, respectively).

Dietary exposure to BaP altered compositions of active gut microbiomes (Fig. 2B). Proportions of *Barnesiellaceae* and *Bacteroidaceae* were significantly less in the 1000 μg g⁻¹ groups relative to the control group (Dunnett test, $p < 0.001$, $p = 0.005$, respectively). The proportion of *Barnesiellaceae* was greater in the 100 μg g⁻¹ group relative to the control group ($p = 0.02$), while the proportion of *Chromobacteriaceae* was significantly less in the 100 μg g⁻¹ group relative to the control group ($p = 0.004$). The proportion of *Flavobacteriaceae* was significantly larger in the 1000 μg g⁻¹ groups relative to the control group ($p < 0.001$). *Mycobacteriaceae* was significantly lower in proportion in the 10 μg g⁻¹ ($p = 0.005$) and 100 μg g⁻¹ ($p = 0.002$) groups relative to control; the

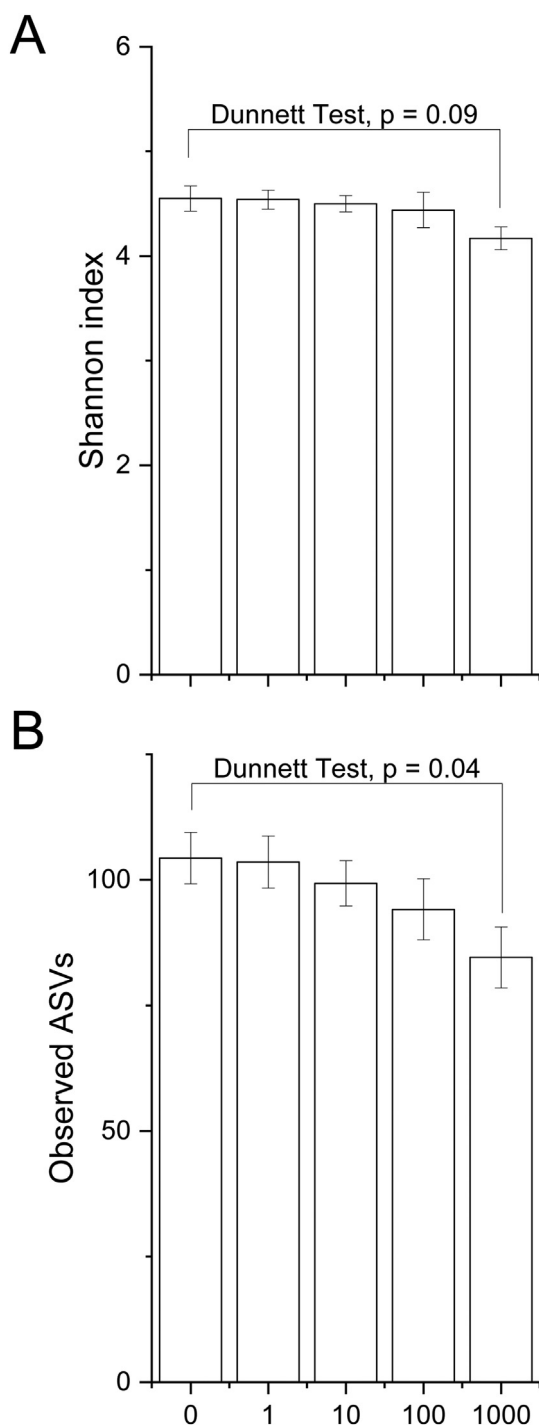


Fig. 1. Shannon Index values and number of observed amplicon sequence variants (ASVs) for each exposure group from the active gut microbiome. Mean and standard error values are presented.

lesser proportion in the 1000 $\mu\text{g g}^{-1}$ group was not significant. Furthermore, several proportions of families (CLR-transformed) were significantly correlated with IgBaP-SO₄ ($p < 0.05$; Fig. S4).

Rare taxa presented greater variance in response to BaP exposure than did more abundant taxa (Fig. S2A–C). The abundant phylum *Actinobacteria* shifted into the rare fraction in 100 $\mu\text{g g}^{-1}$ and 1000 $\mu\text{g g}^{-1}$ groups, and the abundant class *Alphaproteobacteria* shifted into the rare fraction in the 100 $\mu\text{g g}^{-1}$ group. More families shifted between abundant and rare fractions among groups.

The number of nodes and edges of neighborhood selection networks of active microbiomes weren't correlated with exposure dosage (Fig. 3 and Table 1) compared to that of rDNA-based networks (SI Fig. S5 & Table S3). Numbers of nodes and edges were not significantly correlated with concentrations of BaP (Spearman correlation, $P > 0.05$). Edges between ASVs of *Proteobacteria*, *Fusobacteria*, *Bacteroidetes*, or *Actinobacteria* dominated the neighborhood selection networks across groups.

3.3. Concentrations of BaP metabolites correlated with predicted metabolic pathways

In total, 179 MetaCyc pathways of active gut microbiomes were significantly correlated with IgBaP-SO₄ (Spearman correlation, $p < 0.05$, Fig. S6). In total, 22 pathways were negatively correlated with IgBaP-SO₄, while 157 pathways were positively correlated with IgBaP-SO₄. Pathways showed a clear separation among treatment groups, with the control and 1 $\mu\text{g g}^{-1}$ groups clustering together, the 10 and 100 $\mu\text{g g}^{-1}$ groups clustering together, and the 1000 $\mu\text{g g}^{-1}$ group separated from the rest. Several negatively correlated pathways, including super-pathway of fucose and rhamnose degradation, fucose degradation, and mannan degradation were associated with degradations of sugars. A number of positively correlated pathways with IgBaP-SO₄ were associated with the tricarboxylic acid cycle or biosynthesis of amino acids such as methionine, arginine, and tyrosine.

3.4. rDNA-normalized active gut microbiome

The rDNA-normalized active gut microbiome had a better performance to cluster community structure than the genomic or active gut microbiome, corresponding to exposure groups. The rDNA-normalized active gut microbiome showed better separation among exposure groups than the active and genomic gut microbiomes. rDNA-normalized active microbiome (Pseudo-F = 2.0, $p < 0.001$) resulted in greater magnitudes in the structural differences among exposure groups than the genomic (Pseudo-F = 1.4, $p = 0.20$) or active gut microbiome (Pseudo-F = 1.7, $p = 0.03$) (Fig. 4).

rDNA-normalized activity allowed for analysis of the activity-dormancy dynamics of overlapping taxa (Fig. 5). Several proportions of rDNA-normalized active families (CLR-transformed) were significantly correlated with measured IgBaP-SO₄ metabolites (Fig. S4). The normalized active of rare families, *Rikenellaceae*, *Sphingomonadaceae*, *Nocardiaceae*, and *Xanthomonadaceae* were all negatively correlated with IgBaP-SO₄, while that of *Desulfovibrionaceae*, *Microbacteriaceae*, *Flavobacteriaceae*, *Rhizobiaceae*, *Chitinibacteraceae*, and *Moraxellaceae* were positively correlated with IgBaP-SO₄ (Spearman correlation, $p < 0.05$).

rDNA-normalization detected correlations between certain taxa (*Desulfovibrionaceae*, *Shewanellaceae*, *Aeromonadaceae*, *Rhizobiaceae*, and *Nocardiaceae*) and IgBaP-SO₄ that were not observed within the active or genomic microbiomes.

4. Discussion

This study revealed that dietary exposure to BaP significantly altered the active microbiome in the gut of fathead minnows. Genomes of gut microbiota shaped the overall active biodiversity of gut microbiome explored by use of 16S rRNA metabarcoding. The responses of alpha- and beta-diversities of the active microbiome were consistent with that of genomic microbiomes to dietary exposure of BaP. Less abundant and rare taxa of active microbiome had differential compositional responses to BaP exposure from that of genomic microbiome. The use of the rDNA-normalized active microbiome can provide meaningful insights into the hidden impacts of BaP on the microbiome.

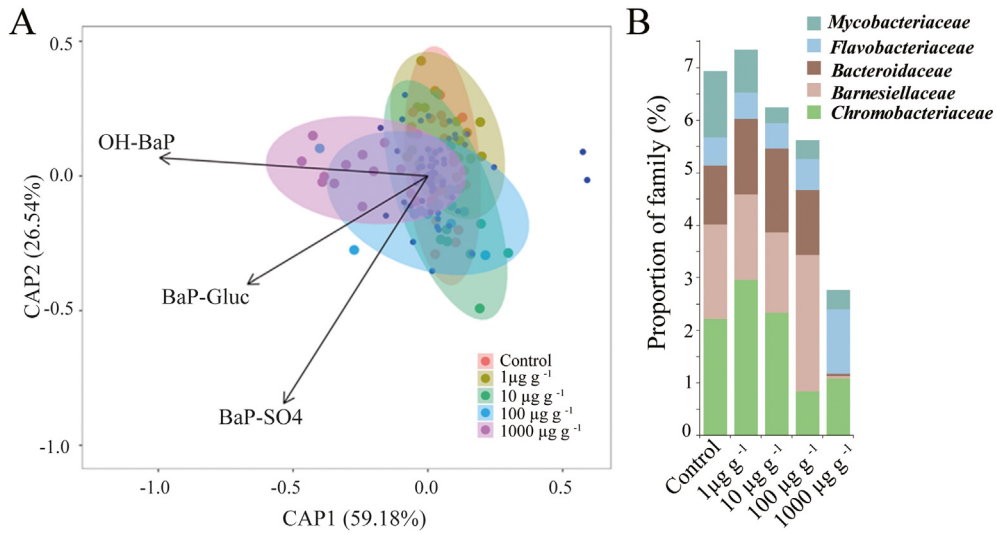


Fig. 2. Families of bacteria from the gut microbiome that were (A) positively and (B) negatively correlated with IgBaP-SO₄ with the genomic, active, and DNA-normalized active microbiomes. (C) Relative abundance of the taxa that were significantly different in the exposure groups relative to the control, based on Dunnett's tests. (D) Constrained Analysis of Principal Coordinates (CAP) of the different exposure groups constrained by the vectors of the measured metabolite concentrations, using Bray-Curtis dissimilarities. Both IgOH-BaP and IgBaP-SO₄ metabolites were the significant environmental variables constraining the ordination ($p = 0.001$ and $p = 0.04$, respectively).

The overall active biodiversity of gut microbiome was shaped by genomic capability of gut microbiota. The abundant active gut microbiome in fathead minnows was consistent with the genomic gut microbiome

from previous studies (DeBofsky et al., 2020; Gaulke et al., 2016; Narowe et al., 2015), but with different proportions. Although the active gut microbiome has similar alpha-diversity as that of genomic gut

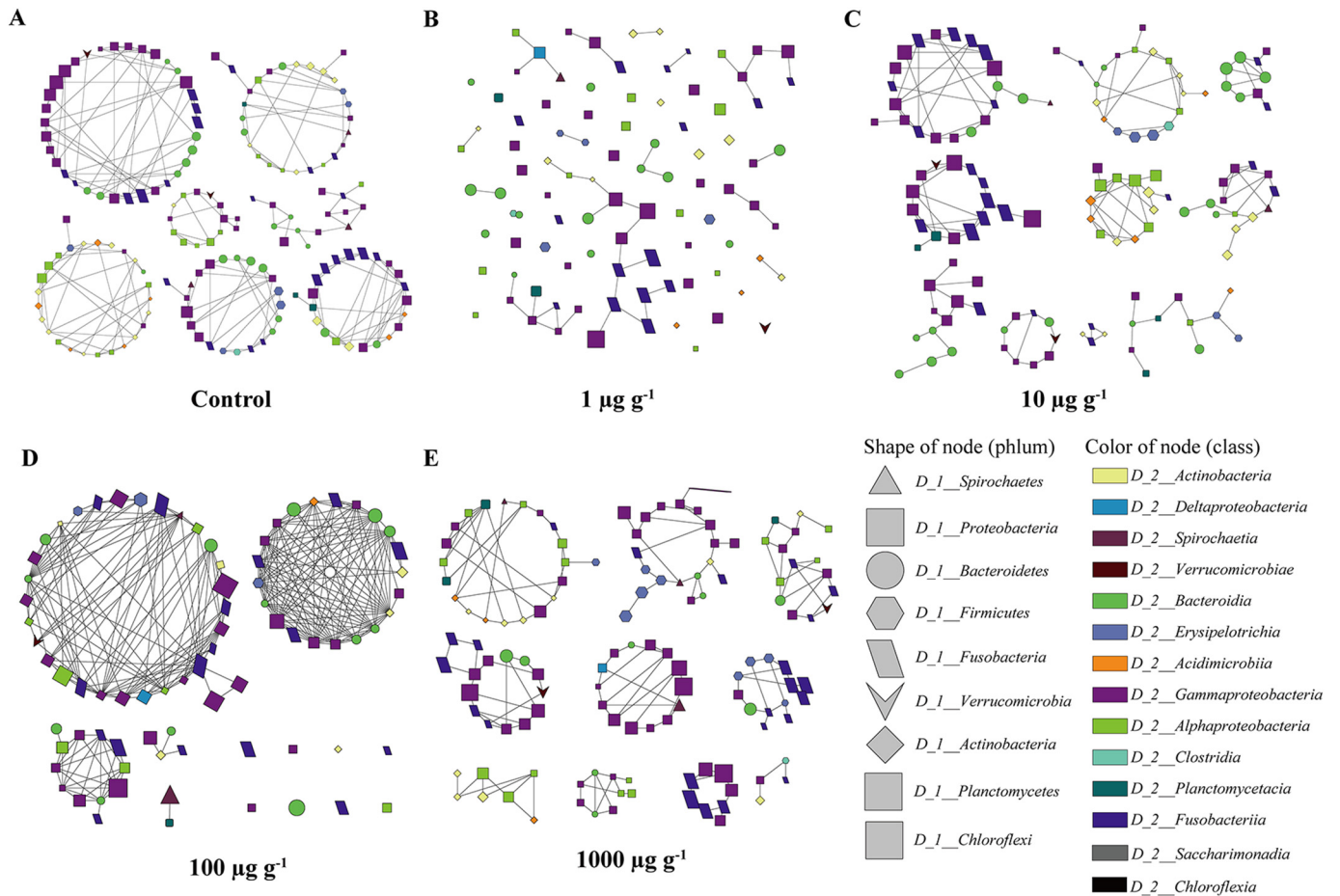


Fig. 3. Neighborhood selection networks of active gut microbiome, as determined with SPIEC-EASI, after exposure to (A) Control, (B) 1, (C) 10, (D) 100, (E) 1000 $\mu\text{g g}^{-1}$ BaP. Shape of node: bacterial phylum; color of node: bacterial class; size of node: abundance.

Table 1
Number of nodes and edges from the neighborhood selection networks of the active gut microbiome.

Group	Number of nodes	Number of nodes (non-alone)	Number of edges	Clustered edges	Percentage of edges <i>Proteobacteria</i> , <i>Fusobacteria</i> , <i>Bacteroidetes</i> , or <i>Actinobacteria</i>
Control	160	160	325	267	82.4%
1 $\mu\text{g g}^{-1}$	94	54	41	40	92.5%
10 $\mu\text{g g}^{-1}$	129	129	205	168	82.7%
100 $\mu\text{g g}^{-1}$	78	68	332	263	75.7%
1000 $\mu\text{g g}^{-1}$	127	127	201	164	76.1%

microbiome (DeBofsky et al., 2021), the composition of active microbiome is different from that of genomic microbiome because a significant portion of gut microbiome might be dormant and not actively transcribing (Jones et al., 2010). The active bacteria with a greater transcript activity might quickly respond to fluctuations in environmental factors or health statuses of hosts (Revetta et al., 2011). Redundancy of gut microbiome might determine bacteria providing similar functions

to have lesser transcript activity (Escalas et al., 2017), which highlights the less-abundant and rare but more active bacteria might be linked to potential nonredundant functions.

Effects of BaP on alpha- and beta-diversity of the gut microbiome were consistent across the active and genomic microbiomes, which suggested the overall responses of gut microbiome to BaP exposure for a short-term is determined by genomic capability of gut microbiota

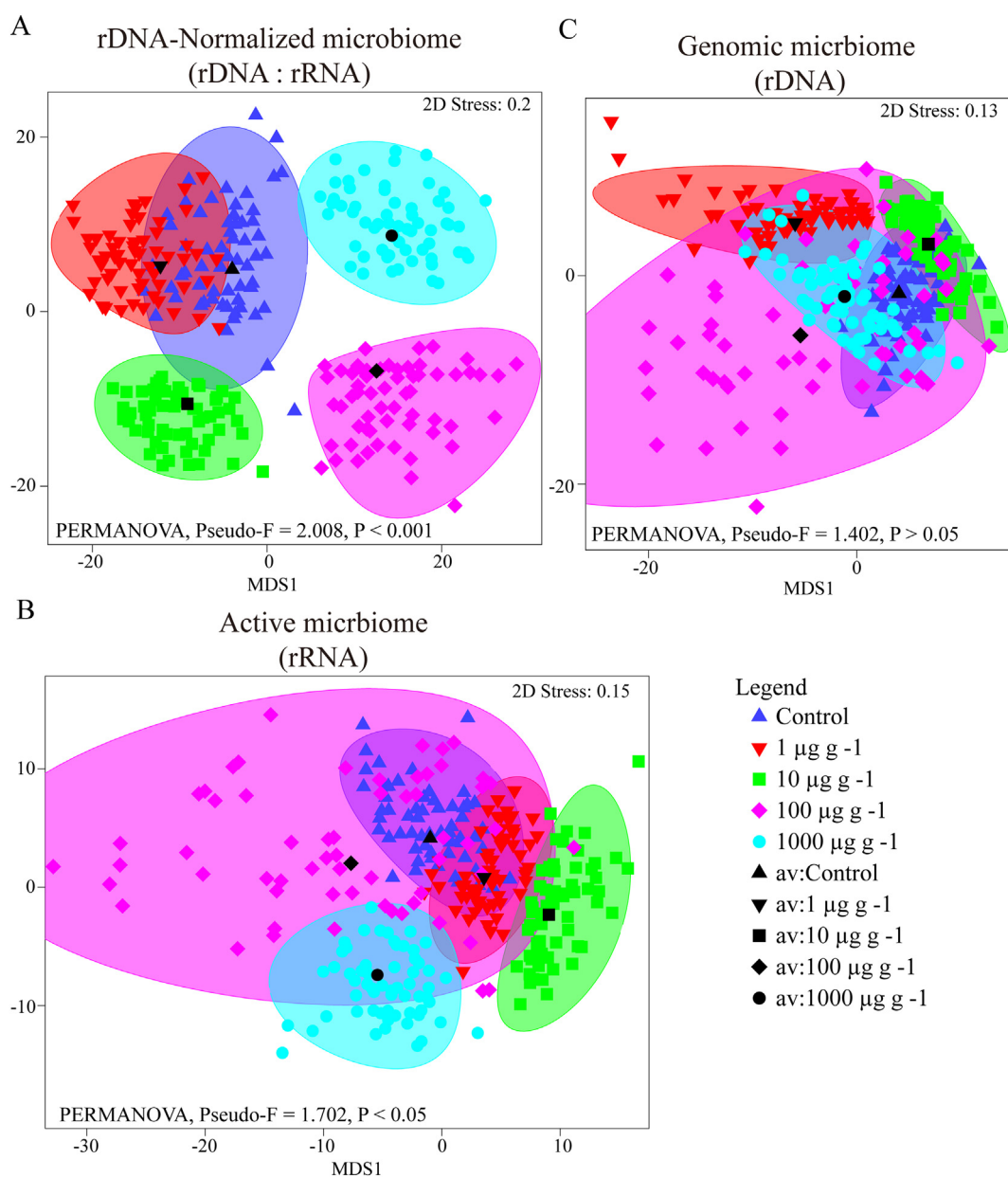


Fig. 4. Bootstrap averages of Metric MDS plot for (A) the DNA-normalized active microbiome, (B) the active microbiome, and (C) the genomic microbiome. ASVs were agglomerated to the genus level. Av: averaged resemblance.

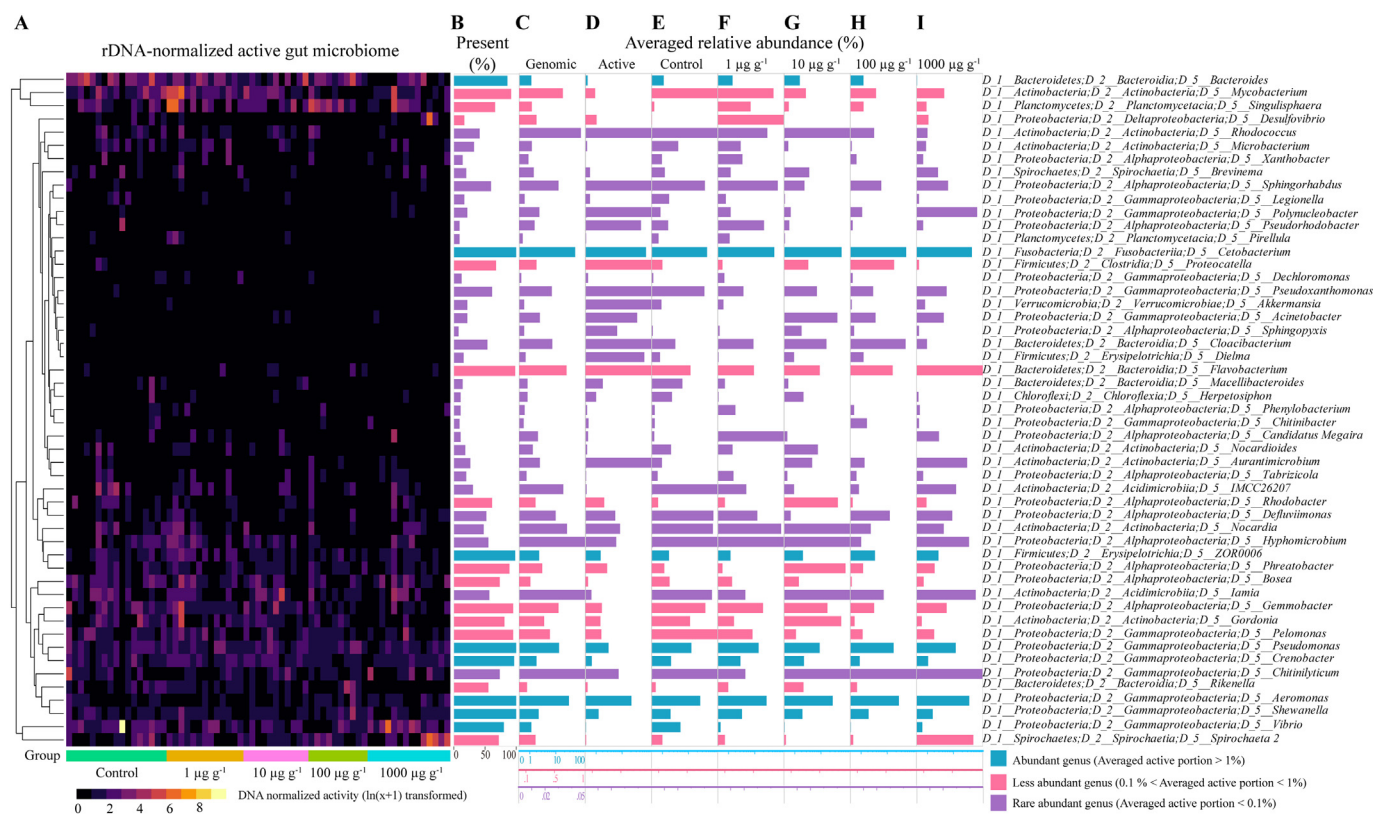


Fig. 5. (A) Heatmap of the abundance of DNA-normalized active gut microbiome in each exposure group. (B) Percent relative abundance of genera across all samples. (D) Percent abundance of genera in the genomic and (D) active microbiomes. (E). Percent relative abundance of genera in the control (F) 1, (G) 10, (H) 100, and (I) 1000 µg g⁻¹ groups. In total, 8 genera were abundant (>1%), shown in blue, 13 genera were less abundant (0.1%–1%), shown in pink, and the remaining 30 genera were rare (<0.1%), shown in purple. (For interpretation of the references to color in this figure legend, the reader is referred to the web version of this article.)

(Madlung and Comai, 2004). Alterations of gut microbiome by BaP might lead to deleterious effects, including decreased digestive function and immune capacity, (Carlson et al., 2004a; Reynaud and Deschaux, 2006). *Bacteroidaceae* and *Barnesiellaceae*, both negatively correlated with IgBaP-SO₄, are associated with digestion (Bäckhed et al., 2005; Ikeda-Ohtsubo et al., 2018; Thomas et al., 2011) and immune regulation (Hiippala et al., 2018). PAH-degrading bacteria are rare in the gut of fish reared under clean lab conditions with lesser concentrations of PAHs in the facilities (Šyovkiene and Mickeniene, 2011). *Moraxellaceae* isolates are capable of degrading BaP (Sowada et al., 2014), while they are recognized as being opportunistic pathogens in fish (Austin and Austin, 2016). PAH-degrading bacteria stimulated by greater concentrations of BaP can result in greater activity (Claus et al., 2016; Ghosal et al., 2016). This supports the conclusion that 16S rRNA metabarcoding is able to detect potentially important rare, but active, taxa that would otherwise be missed with rDNA analyses.

Several taxa in the active microbiome were correlated with IgBaP-SO₄ that were not correlated with taxa inferred from the genomic microbiome. This means that the activity, rather than genomic abundance, of these taxa is either stimulated or inhibited due to exposure to BaP. *Rikenellaceae*, for example, was significantly negatively correlated with IgBaP-SO₄. Exposing mice to the fungicide imazalil resulted in a reduction in proportion of *Rikenellaceae* and was associated with colonic inflammation (Zeng et al., 2016). Reduction in *Rikenellaceae* was also seen in an *in vitro* assay exposing fecal microbiomes to BaP (Defois et al., 2017). Therefore, the reduction in *Rikenellaceae* might be a biomarker of reduced health of these fish. In addition, rRNA metabarcoding exhibited a positive relationship between IgBaP-SO₄ and *Flavobacteriaceae* as well as *Pseudomonadaceae*, which are families that contain known opportunistic pathogens in fish (Austin and Austin, 2016; Loch and Faisal, 2015). Furthermore, there are also a number of bacterial species from *Flavobacteriaceae* and

Pseudomonadaceae that are capable of degrading hydrocarbons (Balba et al., 1998; Šyovkiene and Mickeniene, 2011). The duality of unrelated functions associated with these bacterial families supports the conclusion that exposure to BaP affects abundances of these families. *Burkholderiaceae*, another family positively correlated with IgBaP-SO₄ are also capable of degrading hydrocarbons and are found in greater proportions at contaminated sites (Laurie and Lloyd-Jones, 2000; Seo et al., 2009; Yang et al., 2016). In a study in which mice were exposed to BaP, exposure resulted in a greater proportion of *Alcaligenaceae*, which, are in the order *Burkholderiales* (Ribièrè et al., 2016). Finally, a positive correlation between *Isoosphaeraceae* and fish exposed to BaP via an aqueous exposure was also seen in DeBofsky et al. (2020), although the function of this taxa is uncertain.

Exposure to BaP resulted in reduction in network connectivity and complexity for the genomic (DeBofsky et al., 2021), but not the active microbiomes (this study). Edges between ASVs of *Proteobacteria*, *Fusobacteria* or *Bacteroidetes* of active gut microbiota were resistant to exposure of BaP. Maintenance of the network of the active microbiome across treatments suggests resiliency and resistance of the microbial communities in response to the BaP exposure (Elmqvist et al., 2003). Compared with the network of genomic microbiome, active microbiome had a greater overall complexity, which suggests that the genomic microbiome contains a number of dormant taxa, whereas the active microbiome represents the taxa that are interacting with one another (Blazewicz et al., 2013).

Predicted functions of the active microbiome resulted in more rational patterns of MetaCyc pathways significantly correlated with concentrations of IgBaP-SO₄ than that of the genomic microbiome (DeBofsky et al., 2021). Within the aromatic compound degradation pathways, both predicted 4-methylcatechol degradation (ortho cleavage) and toluene degradation III (aerobic) (via p-cresol) were positively correlated with IgBaP-SO₄. Creatinine degradation was negatively correlated with

IgBaP-SO₄, which is consistent with a previous finding that greater concentrations of creatinine are associated with exposure of humans to PAHs (Srogi, 2007). However, further metagenomics, metatranscriptomics and single-cell metabolomics are required to evaluate complex functions of gut microbiota.

rDNA-normalization of the active microbiome revealed hidden patterns of responses of the gut microbiome exposed to BaP. rDNA-normalization attempted to discern the active bacteria from overall community composition. A large value for normalized activity indicates a certain taxa is more active relative to its abundance, whereas a small value indicates that a taxa is largely dormant (Blazewicz et al., 2013). *Desulfovibrionaceae*, which was correlated with pro-inflammatory phenotypes, was more active at greater dietary exposure to BaP. That result is consistent to that observed in mice exposed to 2,3,7,8-tetrachlorodibenzo-*p*-dioxin (TCDD) (Lefever et al., 2016). Enrichment of the family *Microbacteriaceae* has also been associated with soil sites contaminated with hydrocarbons (Jacques et al., 2007). The families *Shewanellaceae* and *Aeromonadaceae* contain known pathogens (Austin and Austin, 2016), and *Shewanellaceae* is negatively correlated with neutrophil recruitment (Rolig et al., 2015). Greater activity of those taxa may be modulating the immune response along with the BaP exposure. Normalized activity of *Sphingomonadaceae* and *Nocardiaceae* were negatively correlated with IgBaP-SO₄; several members of these families are capable of degrading hydrocarbons (Juhász and Naidu, 2000). Certain genera within *Nocardiaceae* are also pathogenic in fish (Austin and Austin, 2016). While other potential hydrocarbon-degraders and pathogens increased in proportion with increasing concentrations of IgBaP-SO₄, these taxa became dormant as concentrations increased. The dormancy implies that other taxa have a competitive advantage when exposed to BaP (Blazewicz et al., 2013). Several of these taxa correlated with IgBaP-SO₄ metabolites are the least abundant, indicating that rarer taxa are responsible for regulating the response to an exposure to BaP.

5. Conclusions

Active gut microbiome had distinct compositional responses of less abundant and rare taxa to BaP exposure. The results of this study show that exclusively analyzing the genomic or active microbiome study might fail to detect relationships between bacterial proportion and a particular stressor. Not all taxa in the genomic microbiome might be active, but this pool of species represents a potential “seed bank” that can become active at any time, conferring advantage for rapid adaptation to change (Caporaso et al., 2012; İnceoğlu et al., 2015). The rDNA-normalized microbiome might be a better indicator of the response to a stressor, but the issue of “phantom microbes” that are present in the active microbiome but not the genomic microbiome complicate solely relying on rDNA-normalized analyses (Bowsheer et al., 2019). The issue of how to handle these taxa has not been resolved and therefore the importance of these taxa is unknown (Bowsheer et al., 2019). While this study showed that 16S rRNA metabarcoding can address differences between the abundant and rare microbiome, utilization of multiple techniques such as emerging single-cell-omics and gastrointestinal models is necessary to fully understand the complexity of microbial ecosystems.

CRedit authorship contribution statement

Abigail DeBofsky: Investigation, Methodology, Data curation, Writing – original draft. **Yuwei Xie:** Conceptualization, Methodology, Validation, Writing – review & editing. **Jonathan K. Challis:** Resources, Data curation, Writing – review & editing. **Phillip J. Ankley:** Writing – review & editing. **Markus Brinkmann:** Writing – review & editing. **Paul D. Jones:** Funding acquisition, Writing – review & editing. **John P. Giesy:** Conceptualization, Project administration, Funding acquisition, Writing – review & editing.

Declaration of competing interest

The authors declare that they have no known competing financial interests or personal relationships that could have appeared to influence the work reported in this paper.

Acknowledgements

Funding was provided by “Next generation solutions to ensure healthy water resources for future generations” funded by the Global Water Futures program, Canada First Research Excellence Fund (#419205). Dr. Brinkmann was also supported through the Global Water Futures program. Dr. Challis was funded by the Banting Post-Doctoral Fellowship. Prof. Giesy was supported by the Canada Research Chairs Program of the Natural Sciences and Engineering Research Council of Canada (NSERC).

Appendix A. Supplementary data

Rarefaction curve of Shannon indices values across sequencing depths (Fig. S1); Compositions of active gut microbiomes of fathead minnows exposed to benzo[*a*]pyrene (Fig. S2); Venn plot of genus characterized by rDNA and rRNA metabarcoding and PCoA plot of log-transformed Bray-Curtis dissimilarities of 16S rDNA and rRNA metabarcoding (Fig. S3); Genomic, active and rDNA-normalized active families from the microbiome that are significantly correlated with log-transformed BaP-SO₄, along with the correlation values (Fig. S3); Neighborhood selection networks of the genomic gut microbiome from exposure to Control, 1, 10, 100, and 1000 µg g⁻¹ BaP (Fig. S4); Heatmap of the MetaCyc pathways that are significantly correlated with IgBaP-SO₄ at each of the exposure concentrations (Fig. S5); Concentration of food and BaP metabolites along with respective standard errors for the different exposure groups (Table S1); The counts of sequenced, filtered, denoised, merged, non-chimeric, and bacteria only reads for each sample (Table S2); Number of nodes and edges from the neighborhood selection networks of the genomic gut microbiome discovered by rDNA metabarcoding (Table S3). Supplementary data to this article can be found online at <https://doi.org/10.1016/j.scitotenv.2021.151060>.

References

- Abu-Ali, G.S., Mehta, R.S., Lloyd-Price, J., Mallick, H., Branck, T., Ivey, K.L., Drew, D.A., Dulong, C., Rimm, E., Izard, J., Chan, A.T., Huttenhower, C., Chan, H.T.H., 2018. Metatranscriptome of human fecal microbial communities in a cohort of adult men HHS public access. *Nat. Microbiol.* 3, 356–366. <https://doi.org/10.1038/s41564-017-0084-4>.
- Adamovsky, O., Buerger, A., Wormington, A.M., Ector, N., Griffitt, R.J., Bisesi, J.H., Martyniuk, C.J., 2018. The gut microbiome and aquatic toxicology: an emerging concept for environmental health. *Environ. Toxicol. Chem.* <https://doi.org/10.1002/etc.4249>.
- Antwis, R.E., Edwards, K.L., Unwin, B., Walker, S.L., Shultz, S., 2019. Rare gut microbiota associated with breeding success, hormone metabolites and ovarian cycle phase in the critically endangered eastern black rhino. *Microbiome* 7, 27. <https://doi.org/10.1186/s40168-019-0639-0>.
- Austin, B., Austin, D.A., 2016. Bacterial fish pathogens. *Bacterial Fish Pathogens*, Sixth. ed Springer. <https://doi.org/10.1007/978-1-4020-6069-4>.
- Bäckhed, F., Ley, R.E., Sonnenburg, J.L., Peterson, D.A., Gordon, J.I., 2005. Host-bacterial mutualism in the human intestine. *Science* (80-.) <https://doi.org/10.1126/science.1104816>.
- Balba, M.T., Al-Awadhi, N., Al-Daher, R., 1998. Bioremediation of oil-contaminated soil: microbiological methods for feasibility assessment and field evaluation. *J. Microbiol. Methods* 32, 155–164. [https://doi.org/10.1016/S0167-7012\(98\)00020-7](https://doi.org/10.1016/S0167-7012(98)00020-7).
- Beyer, J., Jonsson, G., Porte, C., Krahn, M.M., Ariese, F., 2010. Analytical methods for determining metabolites of polycyclic aromatic hydrocarbon (PAH) pollutants in fish bile: a review. *Environ. Toxicol. Pharmacol.* 30, 224–244. <https://doi.org/10.1016/j.etap.2010.08.004>.
- Blazewicz, S.J., Barnard, R.L., Daly, R.A., Firestone, M.K., 2013. Evaluating rRNA as an indicator of microbial activity in environmental communities: limitations and uses. *ISME J.* <https://doi.org/10.1038/ismej.2013.102>.
- Bolyen, E., Rideout, J.R., Dillon, M.R., Bokulich, N.A., Abnet, C.C., Al-Ghalith, G.A., Alexander, H., Alm, E.J., Arumugam, M., Asnicar, F., Bai, Y., Bisanz, J.E., Bittinger, K., Brejnrod, A., Brislawn, C.J., Brown, C.T., Callahan, B.J., Caraballo-Rodríguez, A.M., Chase, J., Cope,

- E.K., Da Silva, R., Diener, C., Dorresteijn, P.C., Douglas, G.M., Durall, D.M., Duvallet, C., Edwardson, C.F., Ernst, M., Estaki, M., Fouquier, J., Gauglitz, J.M., Gibbons, S.M., Gibson, D.L., Gonzalez, A., Gorlick, K., Guo, J., Hillmann, B., Holmes, S., Holste, H., Huttenhower, C., Huttley, G.A., Janssen, S., Jarmusch, A.K., Jiang, L., Kaehler, B.D., Kang, K.B., Keefe, C.R., Keim, P., Kelley, S.T., Knights, D., Koester, I., Kosciolk, T., Kreps, J., Langille, M.G.L., Lee, J., Ley, R., Liu, Y.X., Löffel, E., Lozupone, C., Maher, M., Marotz, C., Martin, B.D., McDonald, D., McIver, L.J., Melnik, A.V., Metcalf, J.L., Morgan, S.C., Morton, J.T., Naimey, A.T., Navas-Molina, J.A., Nothias, L.F., Orphanian, S.B., Pearson, T., Peoples, S.L., Petras, D., Preuss, M.L., Pruesse, E., Rasmussen, L.B., Rivers, A., Robeson, M.S., Rosenthal, P., Segata, N., Shaffer, M., Shiffer, A., Sinha, R., Song, S.J., Spear, J.R., Swafford, A.D., Thompson, L.R., Torres, P.J., Trinh, P., Tripathi, A., Turnbaugh, P.J., Ul-Hasan, S., van der Hooft, J.J.J., Vargas, F., Vázquez-Baeza, Y., Vogtmann, E., von Hippel, M., Walters, W., Wan, Y., Wang, M., Warren, J., Weber, K.C., Williamson, C.H.D., Willis, A.D., Xu, Z.Z., Zaneveld, J.R., Zhang, Y., Zhu, Q., Knight, R., Caporaso, J.G., Guerrini, C.J., Botkin, J.R., McGuire, A.L., 2019. Reproducible, interactive, scalable and extensible microbiome data science using QIIME 2. *Nat. Biotechnol.* 37, 850–852. <https://doi.org/10.1038/s41587-019-0190-3>.
- Bowsher, A.W., Kearns, P.J., Shade, A., 2019. 16S rRNA/rRNA gene ratios and cell activity staining reveal consistent patterns of microbial activity in plant-associated soil. *mSystems* 4, 1–14. <https://doi.org/10.1128/msystems.00003-19>.
- Campbell, B.J., Yu, L., Heidelberg, J.F., Kirchman, D.L., 2011. Activity of abundant and rare bacteria in a coastal ocean. *Proc. Natl. Acad. Sci. U. S. A.* 108, 12776–12781. <https://doi.org/10.1073/pnas.1101405108>.
- Caporaso, J.G., Paszkiewicz, K., Field, D., Knight, R., Gilbert, J.A., 2012. The Western English Channel contains a persistent microbial seed bank. *ISME J.* 6, 1089–1093. <https://doi.org/10.1038/ismej.2011.162>.
- Carding, S., Verbeke, K., Vipond, D.T., Corfe, B.M., Owen, L.J., 2015. Dysbiosis of the gut microbiota in disease. *Microb. Ecol. Health Dis.* 26, 26191. <https://doi.org/10.3402/mehd.v26.26191>.
- Carlson, E.A., Li, Y., Zelikoff, J.T., 2004a. Benzo[a]pyrene-induced immunotoxicity in Japanese medaka (*Oryzias latipes*): relationship between lymphoid CYP1A activity and humoral immune suppression. *Toxicol. Appl. Pharmacol.* 201, 40–52. <https://doi.org/10.1016/j.taap.2004.04.018>.
- Carlson, E.A., Li, Y., Zelikoff, J.T., 2004b. Suppressive effects of benzo[a]pyrene upon fish immune function: evolutionarily conserved cellular mechanisms of immunotoxicity. *Mar. Environ. Res.* 731–734. <https://doi.org/10.1016/j.marenvres.2004.03.023>.
- Caspi, R., Billington, R., Fulcher, C.A., Keseler, I.M., Kothari, A., Krummenacker, M., Latendresse, M., Midford, P.E., Ong, Q., Ong, W.K., Paley, S., Subhraveti, P., Karp, P.D., 2017. The MetaCyc database of metabolic pathways and enzymes. *Nucleic Acids Res.* 46, 633–639. <https://doi.org/10.1093/nar/gkx935>.
- Chen, J., Wright, K., Davis, J.M., Jeraldo, P., Marietta, E.V., Murray, J., Nelson, H., Matteson, E.L., Taneja, V., 2016. An Expansion of Rare Lineage Intestinal Microbes Characterizes Rheumatoid Arthritis. <https://doi.org/10.1186/s13073-016-0299-7>.
- Claissé, D., 1989. Chemical contamination of french coasts. *Mar. Pollut. Bull.* 20, 523–528.
- Claus, S.P., Guillou, H., Ellero-Simatos, S., 2016. The gut microbiota: a major player in the toxicity of environmental pollutants? *NPJ Biofilms Microbiomes* 2, 16003. <https://doi.org/10.1038/npjbiofilms.2016.3>.
- Costa, J., Ferreira, M., Rey-Salgueiro, L., Reis-Henriques, M.A., 2011. Comparison of the waterborne and dietary routes of exposure on the effects of Benzo(a)pyrene on bio-transformation pathways in Nile tilapia (*Oreochromis niloticus*). *Chemosphere* 84, 1452–1460.
- De Vrieze, J., Regueiro, L., Props, R., Vilchez-Vargas, R., Jáuregui, R., Pieper, D.H., Lema, J.M., Carballa, M., Vilchez-Vargas, R., Jáuregui, R., Pieper, D.H., Lema, J.M., Carballa, M., Vilchez-Vargas, R., Jáuregui, R., Pieper, D.H., Lema, J.M., Carballa, M., 2016. Presence does not imply activity: DNA and RNA patterns differ in response to salt perturbation in anaerobic digestion. *Biotechnol. Biofuels* 9, 244. <https://doi.org/10.1186/s13068-016-0652-5>.
- DeBofsky, A., Xie, Y., Grimard, C., Alcaraz, J., Brinkmann, M., Hecker, M., Giesy, J.P., 2020. Differential responses of gut microbiota of male and female fathead minnow (*Pimephales promelas*) to a short-term environmentally-relevant, aqueous exposure to benzo[a]pyrene. *Chemosphere* 252, 126461. <https://doi.org/10.1016/j.chemosphere.2020.126461>.
- DeBofsky, A., Xie, Y., Challis, J.K., Jain, N., Brinkmann, M., Jones, P.D., Giesy, J.P., 2021. Responses of juvenile fathead minnow (*Pimephales promelas*) gut microbiome to a chronic dietary exposure of benzo[a]pyrene. *Environ. Pollut.* 278, 116821. <https://doi.org/10.1016/j.envpol.2021.116821>.
- Defois, C., Ratel, J., Denis, S., Batut, B., Beugnot, R., Peyretailade, E., Engel, E., Peyret, P., Poretzky, R.S., Nelson, W.C., Herbst, F.-A., Peyret, P., Defois, C., Ratel, J., Denis, S., Batut, B., Beugnot, R., Peyretailade, E., Engel, E., 2017. Environmental pollutant Benzo[a]Pyrene impacts the volatile metabolome and transcriptome of the human gut microbiota. *Front. Microbiol.* 8, 1–12. <https://doi.org/10.3389/fmicb.2017.01562>.
- Dimitroglou, A., Merrifield, D.L., Carnevali, O., Picchiatti, S., Avella, M., Daniels, C., Güroy, D., Davies, S.J., 2011. Microbial manipulations to improve fish health and production - a Mediterranean perspective. *Fish Shellfish Immunol.* <https://doi.org/10.1016/j.fsi.2010.08.009>.
- Douglas, G.M., Maffei, V.J., Zaneveld, J., Yurgel, S.N., Brown, J.R., Taylor, C.M., Huttenhower, C., Langille, M.G.L., 2019. PICRUSt2: An Improved and Extensible Approach for Metagenome Inference. *bioRxiv*, p. 672295. <https://doi.org/10.1101/672295>.
- Egerton, S., Culloty, S., Whooley, J., Stanton, C., Ross, R.P., 2018. The gut microbiota of marine fish. *Front. Microbiol.* <https://doi.org/10.3389/fmicb.2018.00873>.
- Elmqvist, T., Folke, C., Nyström, M., Peterson, G., Bengtsson, J., Walker, B., Norberg, J., 2003. Response diversity, ecosystem change, and resilience. *Front. Ecol. Environ.* 1, 488–494. [https://doi.org/10.1890/1540-9295\(2003\)001\[0488:RDECAR\]2.0.CO;2](https://doi.org/10.1890/1540-9295(2003)001[0488:RDECAR]2.0.CO;2).
- Escalas, A., Troussellier, M., Yuan, T., Bouvier, T., Bouvier, C., Mouchet, M.A., Hernandez, D.F., Miranda, J.R., Zhou, J., Moullot, D., 2017. Functional diversity and redundancy across fish gut, sediment and water bacterial communities. *Environ. Microbiol.* 19, 3268–3282. <https://doi.org/10.1111/1462-2920.13822>.
- Fernandes, A.D., Macklaim, J.M., Linn, T.G., Reid, G., Gloor, G.B., 2013. ANOVA-like differential expression (ALDEx) analysis for mixed population RNA-seq. *PLoS One* 8, e70119.
- Fois, C.A.M., Le, T.Y.L., Schindeler, A., Naficy, S., McClure, D.D., Read, M.N., Valtchev, P., Khademhosseini, A., Dehghani, F., 2019. Models of the gut for analyzing the impact of food and drugs. *Adv. Healthc. Mater.* 8, 1900968. <https://doi.org/10.1002/ADHM.201900968>.
- Gaulke, C.A., Barton, C.L., Proffitt, S., Tanguay, R.L., Sharpton, T.J., 2016. Triclosan exposure is associated with rapid restructuring of the microbiome in adult zebrafish. *PLoS One* 11, 1–20. <https://doi.org/10.1371/journal.pone.0154632>.
- Ghosal, D., Ghosh, S., Dutta, T.K., Ahn, Y., 2016. Current state of knowledge in microbial degradation of polycyclic aromatic hydrocarbons (PAHs): a review. *Front. Microbiol.* <https://doi.org/10.3389/fmicb.2016.01369>.
- Givens, C., Ransom, B., Bano, N., Hollibaugh, J., 2015. Comparison of the gut microbiomes of 12 bony fish and 3 shark species. *Mar. Ecol. Prog. Ser.* 209–223. <https://doi.org/10.3354/meps11034>.
- He, X., Qi, Z., Hou, H., Qian, L., Gao, J., Zhang, X.-X., 2019. Structural and Functional Alterations of Gut Microbiome in Mice Induced by Chronic Cadmium Exposure. <https://doi.org/10.1016/j.chemosphere.2019.125747>.
- Hiippala, K., Jouhten, H., Ronkainen, A., Hartikainen, A., Kainulainen, V., Jalanka, J., Satokari, R., 2018. The potential of gut commensals in reinforcing intestinal barrier function and alleviating inflammation. *Nutrients* 10. <https://doi.org/10.3390/nu10080988>.
- Ikedá-Ohtsubo, W., Brugman, S., Warden, C.H., Rebel, J.M.J., Folkerts, G., Pieterse, C.M.J., 2018. How can we define “optimal microbiota”? A comparative review of structure and functions of microbiota of animals, fish, and plants in agriculture. *Front. Nutr.* <https://doi.org/10.3389/fnut.2018.00090>.
- İnceoğlu, Ö., Lirios, M., Crowe, S.A., García-Armisen, T., Morana, C., Darchambeau, F., Borges, A.V., Descy, J.P., Servais, P., 2015. Vertical distribution of functional potential and active microbial communities in meromictic Lake Kivu. *Microb. Ecol.* 70, 596–611. <https://doi.org/10.1007/s00248-015-0612-9>.
- Jacques, R.J.S., Okeke, B.C., Bento, F.M., Peralba, M.C.R., Camargo, F.A.O., 2007. Characterization of a polycyclic aromatic hydrocarbon-degrading microbial consortium from a petrochemical sludge landfarming site. *Bioremediat. J.* 11, 1–11. <https://doi.org/10.1080/10889860601185822>.
- Jones, S.E., Lennon, J.T., Kellogg, W.K., 2010. Dormancy contributes to the maintenance of microbial diversity. *PNAS* 107, 5881–5886. <https://doi.org/10.1073/pnas.0912765107>.
- Jousset, A., Bienhold, C., Chatzinotas, A., Gallien, L., Gobet, A., Kurm, V., Küsel, K., Rillig, M.C., Rivett, D.W., Salles, J.F., Van Der Heijden, M.G.A., Youssef, N.H., Zhang, X., Wei, Z., Hol, G.W.H., 2017. Where less may be more: How the rare biosphere pulls ecosystems strings. *ISME J.* <https://doi.org/10.1038/ismej.2016.174>.
- Juhász, A.L., Naidu, R., 2000. Bioremediation of high molecular weight polycyclic aromatic hydrocarbons: a review of the microbial degradation of benzo[a]pyrene. *International Biodeterioration and Biodegradation*. Elsevier. [https://doi.org/10.1016/S0964-8305\(00\)00052-4](https://doi.org/10.1016/S0964-8305(00)00052-4).
- Knutzen, J., Sortland, B., 1982. Polycyclic aromatic hydrocarbons (PAH) in some algae and invertebrates from moderately polluted parts of the coast of Norway. *Water Res.* 16, 421–428. [https://doi.org/10.1016/0043-1354\(82\)90166-X](https://doi.org/10.1016/0043-1354(82)90166-X).
- Kotas, M.E., Medzhitov, R., 2015. Homeostasis, inflammation, and disease susceptibility. *Cell* 160, 816–827. <https://doi.org/10.1016/j.cell.2015.02.010>.
- Kurtz, Z.D., Müller, C.L., Miraldi, E.R., Littman, D.R., Blaser, M.J., Bonneau, R.A., 2015. Sparse and compositionally robust inference of microbial ecological networks. *PLoS Comput. Biol.* 11. <https://doi.org/10.1371/journal.pcbi.1004226>.
- Laurie, A.D., Lloyd-Jones, G., 2000. Quantification of phnAc and nahAc in contaminated New Zealand soils by competitive PCR. *Appl. Environ. Microbiol.* 66, 1814–1817.
- Lefever, D.E., Xu, J., Chen, Y., Huang, G., Tamas, N., Guo, T.L., 2016. TCDD modulation of gut microbiome correlated with liver and immune toxicity in streptozotocin (STZ)-induced hyperglycemic mice. *Toxicol. Appl. Pharmacol.* 304, 48–58. <https://doi.org/10.1016/j.taap.2016.05.016>.
- Leitão, R.P., Zuanon, J., Villéger, S., Williams, S.E., Baraloto, C., Fortunel, C., Mendonça, F.P., Moullot, D., 2016. Rare species contribute disproportionately to the functional structure of species assemblages. 283, 20160084. <https://doi.org/10.1098/rspb.2016.0084>.
- Llewellyn, M.S., Boutin, S., Hosenifar, S.H., Derome, N., 2014. Teleost microbiomes: the state of the art in their characterization, manipulation and importance in aquaculture and fisheries. *Front. Microbiol.* 5, 1–17. <https://doi.org/10.3389/fmicb.2014.00207>.
- Loch, T.P., Faisal, M., 2015. Emerging flavobacterial infections in fish: a review. *J. Adv. Res.* 6, 283–300. <https://doi.org/10.1016/j.jare.2014.10.009>.
- Madlung, A., Comai, L., 2004. The effect of stress on genome regulation and structure. *Ann. Bot.* <https://doi.org/10.1093/aob/mch172>.
- Martinez Arbizu, P., 2019. pairwiseAdonis: Pairwise Multilevel Comparison Using Adonis. *R Package Version 0.3*.
- Meinshausen, N., Bühlmann, P., 2006. High-dimensional graphs and variable selection with the lasso. *Ann. Stat.* 34, 1436–1462. <https://doi.org/10.1214/009053606000000281>.
- Nacci, D.E., Kohan, M., Pelletier, M., George, E., 2002. Effects of benzo[a]pyrene exposure on a fish population resistant to the toxic effects of dioxin-like compounds. *Aquat. Toxicol.* 57 (4), 203–215. [https://doi.org/10.1016/S0166-445X\(01\)00196-5](https://doi.org/10.1016/S0166-445X(01)00196-5).
- Narrows, A.B., Albuthi-Lantz, M., Smith, E.P., Bower, K.J., Roane, T.M., Vajda, A.M., Miller, C.S., 2015. Perturbation and restoration of the fathead minnow gut microbiome after low-level triclosan exposure. *Microbiome* 3, 6. <https://doi.org/10.1186/s40168-015-0069-6>.
- Oksanen, J., Blanchet, F.G., Friendly, M., Kindt, R., Legendre, P., McGinn, D., Minchin, P.R., O'Hara, R.B., Simpson, G.L., Solymos, P., Stevens, M.H.H., Szoecs, E., Wagner, H., 2019. *vegan: Community Ecology Package*.

- Pérez, T., Balcázar, J.L., Ruiz-Zarzuola, I., Halaihel, N., Vendrell, D., De Blas, I., Múzquiz, J.L., Múzquiz, J.L., 2010. Host–microbiota interactions within the fish intestinal ecosystem. *Mucosal Immunol.* 3, 355–360. <https://doi.org/10.1038/mi.2010.12>.
- Phalen, L.J., Köllner, B., Leclair, L.A., Hogan, N.S., Van Den Heuvel, M.R., 2014. The effects of benzo[a]pyrene on leucocyte distribution and antibody response in rainbow trout (*Oncorhynchus mykiss*). *Aquat. Toxicol.* 147, 121–128. <https://doi.org/10.1016/j.aquatox.2013.12.017>.
- R Core Team, 2013. R: A language and environment for statistical computing. R Foundation for Statistical Computing, Vienna, Austria. 3.6.1, 2013. <https://www.R-project.org/>.
- Revetta, R.P., Matib, R.S., Santo Domingo, J.W., 2011. 16S rRNA gene sequence analysis of drinking water using RNA and DNA extracts as targets for clone library development. *Curr. Microbiol.* 63, 50–59. <https://doi.org/10.1007/s00284-011-9938-9>.
- Reynaud, S., Deschaux, P., 2006. The effects of polycyclic aromatic hydrocarbons on the immune system of fish: a review. *Aquat. Toxicol.* 77 (2), 229–238. <https://doi.org/10.1016/j.aquatox.2005.10.018> (Elsevier).
- Rivière, C., Peyret, P., Parisot, N., Darcha, C., Déchelotte, P.J., Barnich, N., Peyretailade, E., Boucher, D., 2016. Oral exposure to environmental pollutant benzo[a]pyrene impacts the intestinal epithelium and induces gut microbial shifts in murine model. *Sci. Rep.* 6, 1–11. <https://doi.org/10.1038/srep31027>.
- Rolig, A.S., Parthasarathy, R., Burns, A.R., Bohannon, B.J.M.M., Guillemin, K., Correspondence, K.G., Guillemin, K., Correspondence, K.G., Guillemin, K., Correspondence, K.G., Guillemin, K., 2015. Individual members of the microbiota disproportionately modulate host innate immune responses. *Cell Host Microbe* 18, 613–620. <https://doi.org/10.1016/j.chom.2015.10.009>.
- Sandvik, M., Horsberg, T.E., Skaare, J.U., Ingebrigtsen, K., 1998. Comparison of dietary and waterborne exposure to benzo[a]pyrene: bioavailability, tissue disposition and CYP1A1 induction in rainbow trout (*Oncorhynchus mykiss*). *Biomarkers* 3, 399–410. <https://doi.org/10.1080/135475098231048>.
- Seo, J.S., Keum, Y.S., Li, Q.X., 2009. Bacterial degradation of aromatic compounds. *Int. J. Environ. Res. Public Health.* <https://doi.org/10.3390/ijerph6010278>.
- Sfanos, K.S., Markowski, M.C., Peiffer, L.B., Ernst, S.E., White, J.R., Kenneth, Pienta, J., Antonarakis, E.S., Ross, A.E., 2018. Compositional differences in gastrointestinal microbiota in prostate cancer patients treated with androgen axis-targeted therapies. *Prostate Cancer Prostatic Dis.* 21, 539–548. <https://doi.org/10.1038/s41391-018-0061-x>.
- Sowada, J., Schmalenberger, A., Ebner, I., Luch, A., Tralau, T., 2014. Degradation of benzo[a]pyrene by bacterial isolates from human skin. *FEMS Microbiol. Ecol.* 88, 129–139. <https://doi.org/10.1111/1574-6941.12276>.
- Srogi, K., 2007. Monitoring of environmental exposure to polycyclic aromatic hydrocarbons: a review. *Environ. Chem. Lett.* <https://doi.org/10.1007/s10311-007-0095-0>.
- Šyvokiene, J., Mickeniene, L., 2011. Hydrocarbon-degrading bacteria associated with intestinal tract of fish from the Baltic Sea. *J. Environ. Eng. Landsc. Manag.* 19, 244–250. <https://doi.org/10.3846/16486897.2011.602559>.
- Thomas, F., Hehemann, J.H., Rebuffet, E., Czekaj, M., Michel, G., 2011. Environmental and gut bacteroidetes: the food connection. *Front. Microbiol.* 2. <https://doi.org/10.3389/fmicb.2011.00093>.
- Tuvikene, A., 1995. Responses of fish to polycyclic aromatic hydrocarbons (PAHs). *Annu. Zool. Fenn.* 32, 295–309. <https://doi.org/10.2307/23735700>.
- Van den Abbeele, P., Verstraete, W., El Aidy, S., Geirnaert, A., Van de Wiele, T., 2013. Prebiotics, faecal transplants and microbial network units to stimulate biodiversity of the human gut microbiome. *Microb. Biotechnol.* 6, 335–340. <https://doi.org/10.1111/1751-7915.12049>.
- Vinebrooke, R.D., Cottingham, K.L., Norberg, J., Scheffer, M., Dodson, S.I., Maberly, S.C., Sommer, U., 2004. Impacts of multiple stressors on biodiversity and ecosystem functioning: the role of species co-tolerance. *Oikos*, 451–457. <https://doi.org/10.1111/j.0030-1299.2004.13255.x>.
- Xie, S., Zhou, A., Xu, N., Feng, Y., Pan, Z., Junaid, M., Wang, J., Zou, J., 2020. Benzo[a]pyrene induces microbiome dysbiosis and inflammation in the intestinal tracts of western mosquitofish (*Gambusia affinis*) and zebrafish (*Danio rerio*). *Fish Shellfish Immunol.* 105, 24–34. <https://doi.org/10.1016/j.fsi.2020.06.041>.
- Xu, X., Liu, W., Tian, S., Wang, W., Qi, Q., Jiang, P., Gao, X., Li, F., Li, H., Yu, H., 2018. Petroleum hydrocarbon-degrading bacteria for the remediation of oil pollution under aerobic conditions: a perspective analysis. *Front. Microbiol.* <https://doi.org/10.3389/fmicb.2018.02885>.
- Yang, S., Wen, X., Shi, Y., Liebner, S., Jin, H., Perfumo, A., 2016. Hydrocarbon degraders establish at the costs of microbial richness, abundance and keystone taxa after crude oil contamination in permafrost environments. *Sci. Rep.* 6. <https://doi.org/10.1038/srep37473>.
- Zeng, Z., Jin, C., Fu, Z., Jin, Y., 2016. Oral Imazalil Exposure Induces Gut Microbiota Dysbiosis and Colonic Inflammation in Mice. <https://doi.org/10.13140/RG.2.1.4802.7123>.
- Zhou, Y., Leung, M.H.Y., Tong, X., Lai, Y., Tong, J.C.K., Ridley, I.A., Lee, P.K.H., 2021. Profiling airborne microbiota in mechanically ventilated buildings across seasons in Hong Kong reveals higher metabolic activity in low-abundance bacteria. *Environ. Sci. Technol.* 55, 249–259. <https://doi.org/10.1021/acs.est.0c06201>.

1 **Supplemental Information for**

2 16S rRNA metabarcoding unearths responses of rare gut microbiome of
3 fathead minnows exposed to benzo[a]pyrene

4 Abigail DeBofsky[†], Yuwei Xie^{†*}, Jonathan K. Challis[†], Phillip J. Ankley[†], Markus Brinkmann^{†,‡},
5 Paul D. Jones^{†,‡}, John P. Giesy^{†,§,¥}

6 [†]Toxicology Centre, University of Saskatchewan, Saskatoon, Saskatchewan, Canada

7 [§]Department of Veterinary Biomedical Sciences and Toxicology Centre, University of
8 Saskatchewan, Saskatoon, Saskatchewan, Canada

9 [‡]School of Environment and Sustainability, University of Saskatchewan, Saskatoon,
10 Saskatchewan, Canada

11 [¥]Department of Environmental Science, Baylor University, Waco, Texas, USA

12
13 * Corresponding author at Toxicology Centre, University of Saskatchewan, Saskatoon, S7N 5B3,
14 Saskatchewan, Canada. Tel: +01-306-9664978

15 *E-mail address:* yuwei.xie@usask.ca (YW Xie)

16
17 Summary of the number of supplemental figures and tables: Figures: 6; Tables: 3

18 **CONTENT**

19 **Supplemental Fig. S1:** Rarefaction curve of Shannon indices values across sequencing depths.

20 **Supplemental Fig. S2:** Compositions of active gut microbiomes of fathead minnows exposed to
21 benzo[a]pyrene at the (A) phylum, (B) class, and (C) family level.

22 **Supplemental Fig. S3:** (A) Venn plot of genus characterized by 16S rDNA and rRNA
23 metabarcoding; (B) PCoA plot of log-transformed Bray-Curtis dissimilarities of 16S rDNA and
24 rRNA metabarcoding, shown in red and blue, respectively.

25 **Supplemental Fig. S4:** (A) Genomic (B) Active and (C) rDNA-normalized active families from
26 the microbiome that are significantly correlated with log-transformed BaP-SO₄, along with the
27 correlation values.

28 **Supplemental Fig. S5:** Neighborhood selection networks of the genomic gut microbiome from
29 exposure to (A) Control, (B) 1, (C) 10, (D) 100, and (E) 1000 µg g⁻¹ BaP. Shape of node:
30 bacterial phylum; color of node: bacterial class; Size of node: abundance.

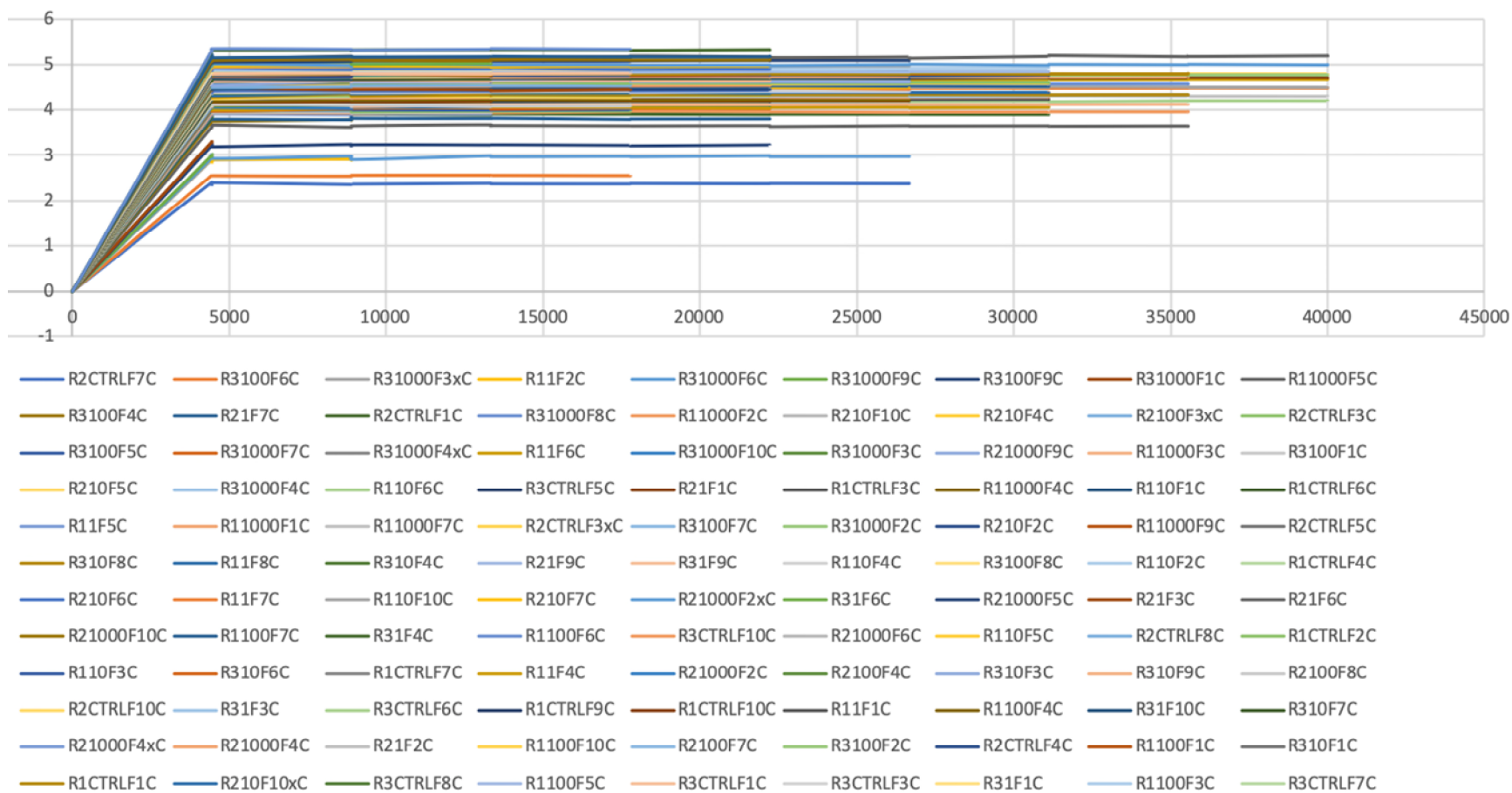
31 **Supplemental Fig. S6:** Heatmap of the MetaCyc pathways that are significantly correlated with
32 lgBaP-SO₄ at each of the exposure concentrations. The correlation value of each pathway with
33 lgBaP-SO₄ is shown on the left. Colors denote a scaled relative abundance for visualization, from
34 the pheatmap package in R, of the MetaCyc pathways, with red indicating more abundant, and
35 yellow indicating less abundant.

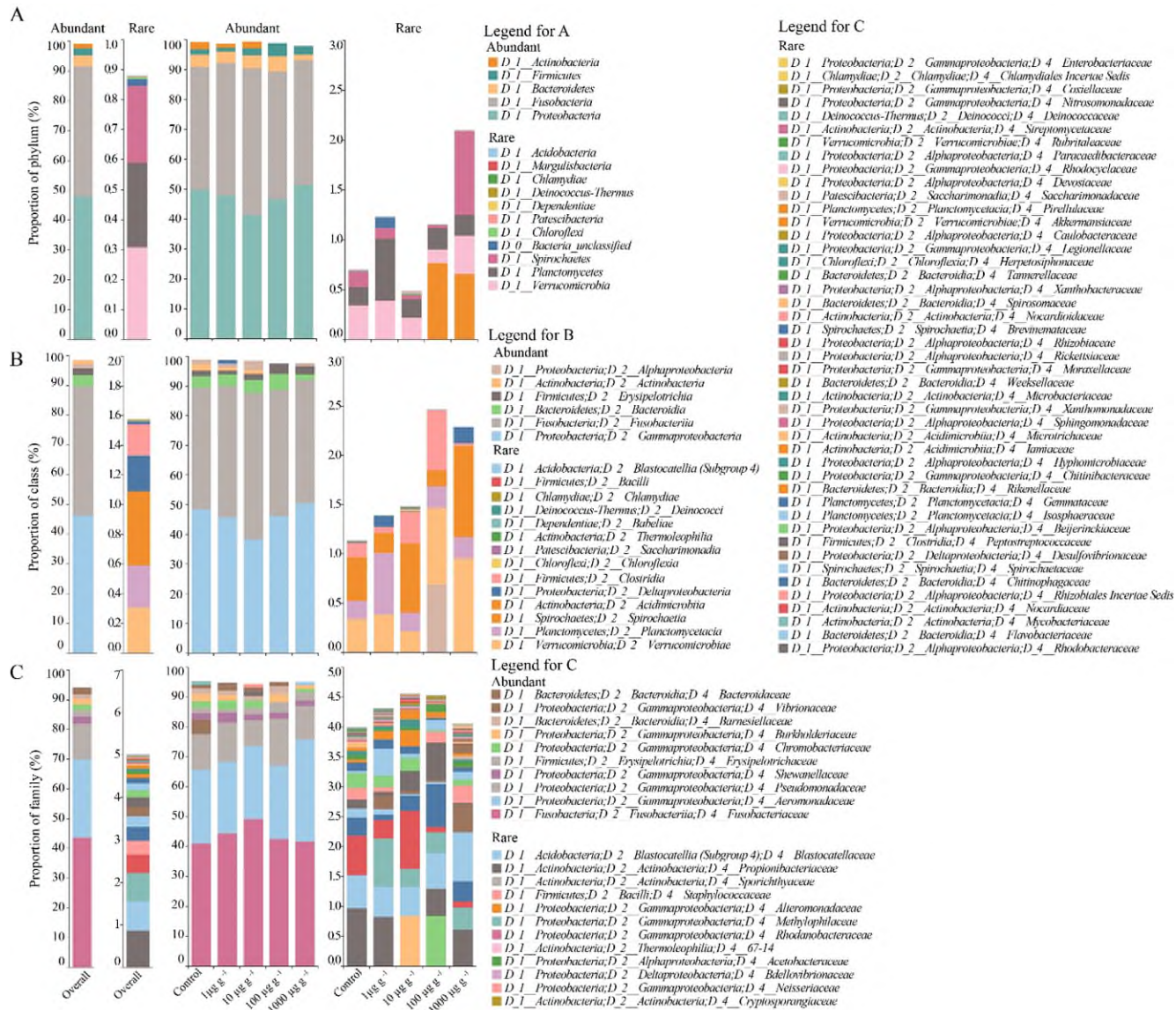
36

37 **Supplemental Table S1:** Concentration of food and BaP metabolites along with respective
38 standard errors for the different exposure groups.

39 **Supplemental Table S2:** The counts of sequenced, filtered, denoised, merged, non-chimeric,
40 and bacteria only reads for each sample.

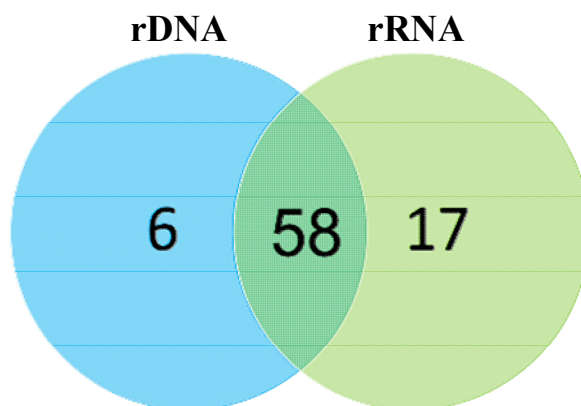
41 **Supplemental Table S3:** Number of nodes and edges from the neighborhood selection networks
42 of the genomic gut microbiome discovered by rDNA metabarcoding.



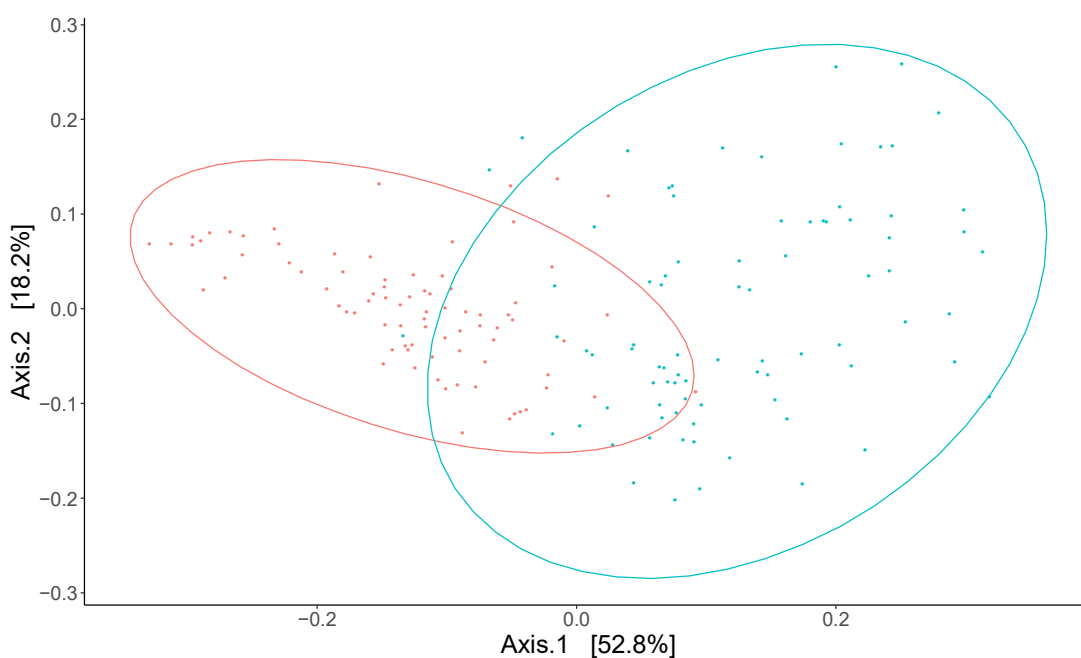


45
46 **Fig. S2:** Compositions of active gut microbiomes of fathead minnows exposed to benzo[a]pyrene at the (A) phylum, (B) class, and (C)
47 family level.

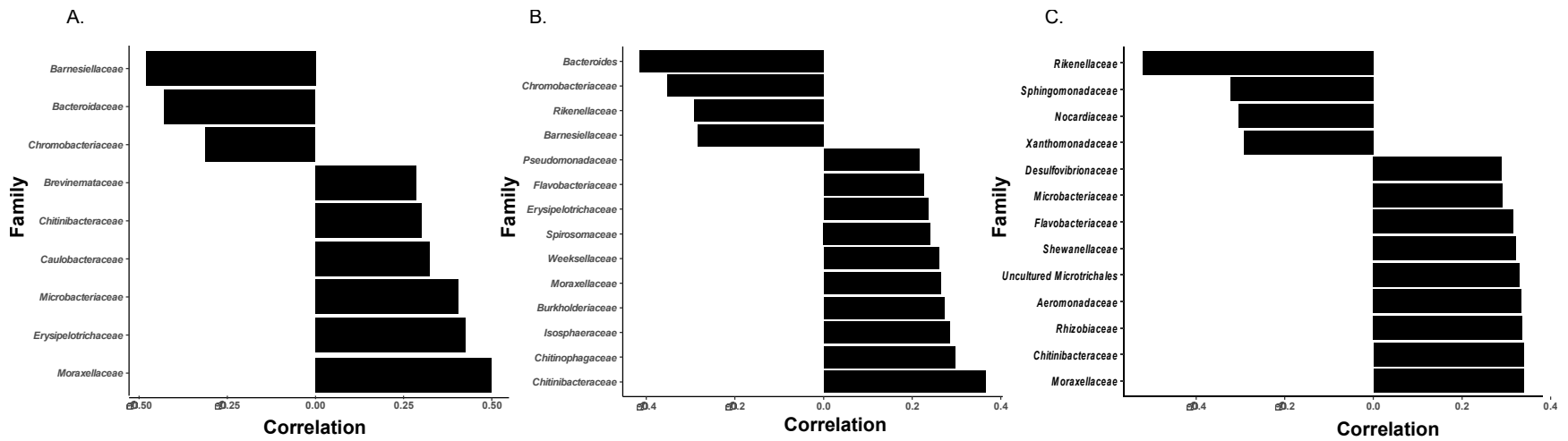
48 A
49



50 B
51

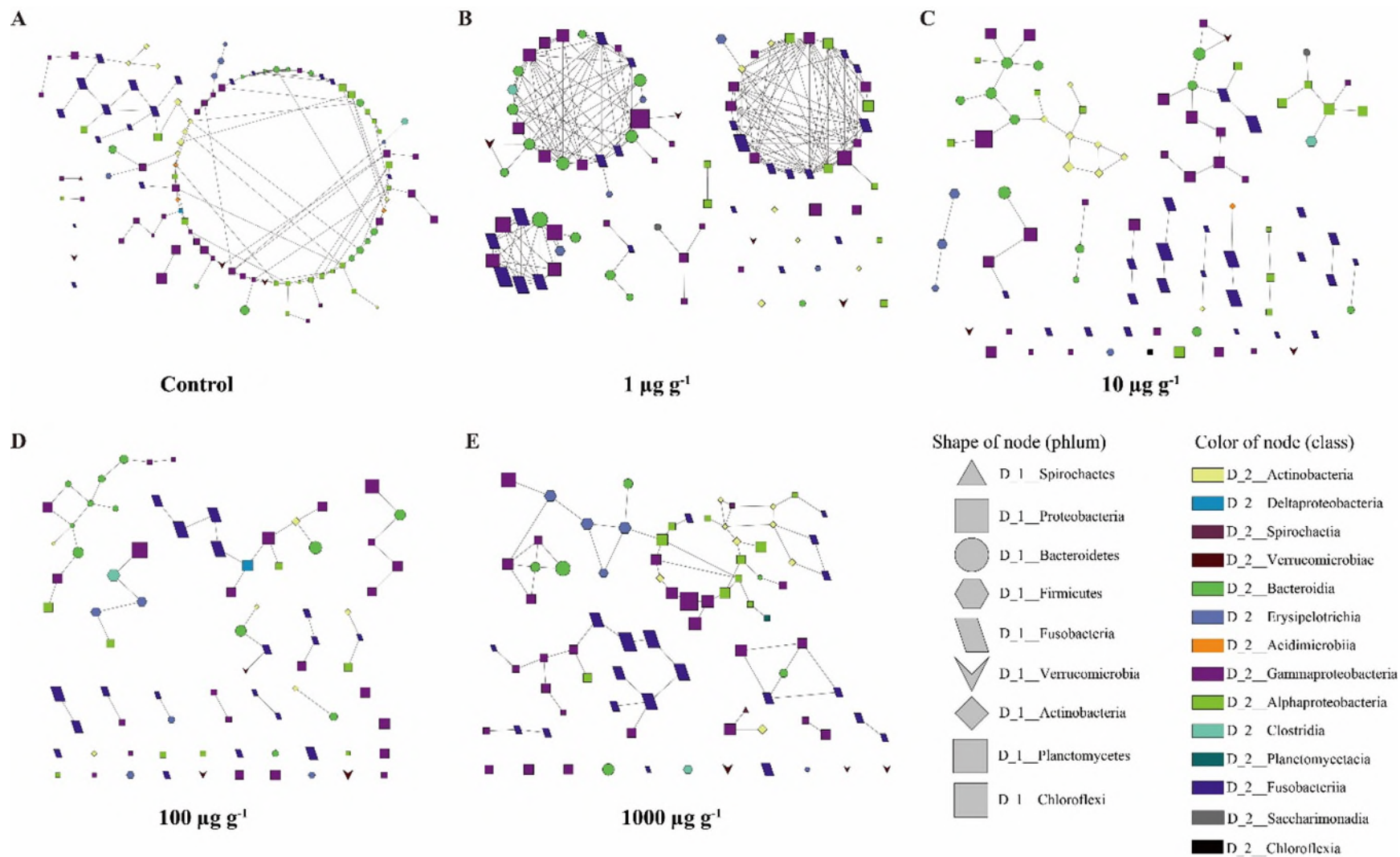


52
53 **Fig. S3:** (A) Venn plot of genus characterized by 16S rDNA and rRNA metabarcoding; (B)
54 PCoA plot of log-transformed Bray-Curtis dissimilarities of 16S rDNA and rRNA
55 metabarcoding, shown in red and blue, respectively.



56
 57 **Fig. S4:** (A) Genomic (B) Active and (C) rDNA-normalized active families from the microbiome that are significantly correlated with
 58 log-transformed BaP-SO₄, along with the correlation values.
 59

60



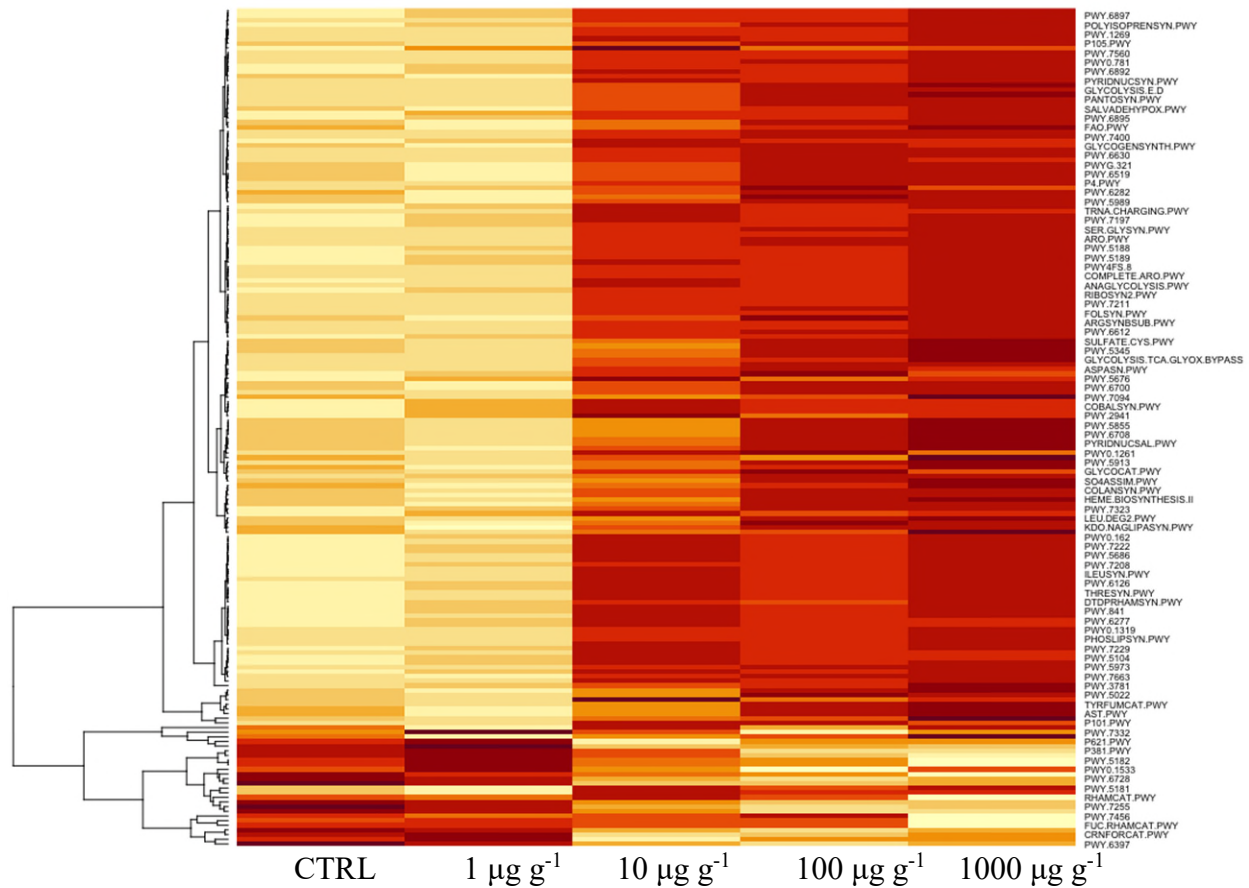
61

62

Fig. S5: Neighborhood selection networks of the genomic gut microbiome from exposure to (A) Control, (B) 1, (C) 10, (D) 100, and

63

(E) 1000 $\mu\text{g g}^{-1}$ BaP. Shape of node: bacterial phylum; color of node: bacterial class; Size of node: abundance.



64
65
66
67
68
69
70
71
72

Fig. S6: Heatmap of the MetaCyc pathways that are significantly correlated with lgBaP-SO₄ at each of the exposure concentrations. The correlation value of each pathway with lgBaP-SO₄ is shown on the left. Colors denote a scaled relative abundance for visualization, from the heatmap package in R, of the MetaCyc pathways, with red indicating more abundant, and yellow indicating less abundant.

73 **Table S1:** Concentration of food and BaP metabolites along with respective standard errors for
74 the different exposure groups.

Exposure ($\mu\text{g g}^{-1}$)	Food ($\mu\text{g g}^{-1}$)	OH-BaP (ng g^{-1})	BaP-Gluc (ng g^{-1})	BaP-SO ₄ (ng g^{-1})
CTRL	0.06 ± 0.02	0	0	178.12 ± 51.28
1	0.98 ± 0.04	0	1.44 ± 1.44	46.67 ± 17.87
10	8.03 ± 1.61	0	9.63 ± 2.88	1385.3 ± 307.71
100	104.61 ± 3.08	7.67 ± 3.32	157.07 ± 46.88	8084.58 ± 2281.28
1000	1166.45 ± 32.07	48.98 ± 16.66	280.35 ± 92.64	41003.53 ± 9556.2

75

76 **Table S2:** The counts of sequenced, filtered, denoised, merged, non-chimeric, and bacteria only
77 reads for each sample.

sample-id	input	filtered	denoised	merged	non-chimeric	bact only
R11000F1C	41391	40661	40018	38155	32565	32539
R11000F2C	44524	43970	43792	43363	40261	39744
R11000F3C	49160	48119	47383	45381	36812	36812
R11000F4C	34808	34108	33681	32416	27072	27057
R11000F5C	53894	53128	52715	50719	40097	39118
R11000F6C	7	6	4	3	3	3
R11000F7C	61653	60684	60077	58006	49835	49703
R11000F9C	47633	46812	46030	43728	34523	34504
R1100F10C	61568	60537	59646	56383	41408	40360
R1100F1C	54401	53459	52329	48760	37757	37725
R1100F2C	5	5	3	0	0	#N/A
R1100F3C	50236	49364	48500	45809	35609	35483
R1100F4C	40079	39424	38632	36128	29070	29042
R1100F5C	45038	44115	43619	41551	34398	34358
R1100F6C	56392	55524	54897	52087	37808	37801
R1100F7C	46141	45461	44828	42785	34480	34471
R1100F8C	36281	35554	34956	32813	25350	25258
R1100F9C	3	1	1	1	1	#N/A
R110F10C	57091	56185	55494	53461	45056	45048
R110F1C	18010	17759	17494	16601	14365	14345
R110F2C	55878	55043	54341	52187	42803	42781
R110F3C	33241	32608	32166	30928	28649	28438
R110F4C	41132	40410	39860	38065	30891	30874
R110F5C	50829	50012	49164	46087	35532	35428
R110F6C	58978	58126	57509	55458	45249	45130
R110F8C	15	13	3	0	0	#N/A
R11F10C	14	14	9	9	4	4
R11F1C	40030	39470	38883	36711	31641	31615
R11F2C	16079	15295	14996	14627	14146	12475
R11F3C	43	43	26	26	26	26
R11F4C	55141	54207	53467	51071	43399	43244
R11F5C	16916	16586	16251	15150	12060	11919
R11F6C	41771	41011	40684	39463	34465	34394
R11F7C	55930	55043	54097	51417	40942	40873
R11F7xC	65	40	32	31	31	31

sample-id	input	filtered	denoised	merged	non-chimeric	bact only
R11F8C	39823	39318	38884	37399	33388	33384
R11F9C	11	11	6	0	0	#N/A
R1CTRLF10C	59382	58454	57659	54854	44361	44304
R1CTRLF1C	51253	50377	49887	47677	39181	39158
R1CTRLF2C	50171	49394	48319	45196	33658	33614
R1CTRLF3C	43047	42464	41891	40344	31932	31904
R1CTRLF4C	47658	46875	46217	43965	34418	34394
R1CTRLF5C	12	12	4	4	4	4
R1CTRLF6C	15899	15674	15336	14468	11601	11601
R1CTRLF7C	12655	12251	11884	11072	9732	9696
R1CTRLF8C	58582	57368	56726	54342	46943	46943
R1CTRLF9C	41067	40460	40153	39134	36947	36853
R21000F10C	36394	35914	35248	33387	30871	29983
R21000F1C	31	30	15	13	13	13
R21000F2C	18683	18365	17886	16345	13265	13237
R21000F2xC	32705	32248	31619	29892	24443	24443
R21000F4C	55913	55152	54201	50599	36175	36008
R21000F4xC	34659	34146	33290	30790	23901	23837
R21000F5C	30559	30105	29647	28017	23855	23838
R21000F6C	34411	33719	33094	30965	25158	25085
R21000F9C	37068	36550	36049	34131	25583	25577
R2100F1C	18539	17887	17312	15656	11293	3698
R2100F2C	20890	20587	20214	18762	12812	#N/A
R2100F3C	26803	26406	25896	24036	17040	17036
R2100F3xC	30099	29674	29193	27662	20053	20000
R2100F4C	28870	28426	27894	26125	18873	18864
R2100F5C	40995	40261	39375	36747	27268	27134
R2100F7C	26568	26176	25530	23659	17333	17292
R2100F8C	8982	8822	8565	7912	6680	6680
R210F10C	21335	21041	20761	19952	17171	15994
R210F10xC	38850	38105	37349	35067	27238	27065
R210F2C	29395	29016	28593	27141	21727	21720
R210F3C	40	38	27	26	26	26
R210F4C	27564	27082	26749	25593	19652	19498
R210F5C	30894	30479	30203	29379	25407	25404
R210F6C	33152	32709	32146	30285	22589	22540
R210F7C	40075	39461	38829	36684	29471	29424
R210F8C	30279	29839	28896	26131	21146	21034
R210F9C	36430	35878	34566	30780	24685	24433

sample-id	input	filtered	denoised	merged	non-chimeric	bact only
R21F10C	30	28	13	11	11	#N/A
R21F1C	38820	38242	37619	35514	27145	27139
R21F2C	25789	25438	24919	23171	17997	17993
R21F3C	23113	22822	22589	21936	21090	20622
R21F5C	39583	38994	38064	35348	29381	29372
R21F6C	34915	34327	33619	31263	22793	22733
R21F7C	32474	31897	31371	30024	25559	25503
R21F8C	34159	33595	32697	29768	22723	22424
R21F9C	36042	35458	34819	32692	27081	27069
R2CTRLF10C	34791	34218	33522	31242	26591	26351
R2CTRLF1C	39431	38939	38703	37961	35014	34839
R2CTRLF2C	33942	33319	32589	30211	25004	24990
R2CTRLF3C	27448	26994	26546	25182	19046	19030
R2CTRLF3xC	31210	30791	30333	29020	20922	20916
R2CTRLF4C	43137	42466	41805	39471	31555	31471
R2CTRLF4xC	31473	30940	29927	26850	21340	21279
R2CTRLF5C	42068	41519	40814	38490	30695	30655
R2CTRLF7C	31967	31582	31359	30997	27427	27162
R2CTRLF8C	30215	29760	28842	26466	21119	21102
R2CTRLF9C	34457	33953	32929	29713	24340	24070
R31000F10C	26306	25977	25258	23668	17306	17294
R31000F1C	8249	8140	7948	7537	6719	6707
R31000F2C	34925	34523	33675	30642	24525	23439
R31000F3C	36637	36206	35494	33445	26726	26423
R31000F3xC	13039	12858	12593	11896	9361	8966
R31000F4C	44859	44311	43566	41105	30841	30794
R31000F4xC	42566	42021	41371	40057	35889	34964
R31000F6C	40860	40354	40042	39090	31464	30926
R31000F7C	36548	36072	35412	33470	24630	24517
R31000F8C	19926	19683	19200	17823	14559	14255
R31000F9C	12049	11826	11596	11079	8387	8240
R3100F1C	25920	25589	24996	23473	18943	18931
R3100F2C	48581	47948	47340	45056	42431	40731
R3100F4C	12608	12407	12250	11880	11722	11309
R3100F5C	27813	27494	26881	25370	19849	19694
R3100F6C	19972	19675	19393	18848	18627	18575
R3100F7C	45992	45242	44540	42714	38492	38113
R3100F8C	13542	13363	12946	11621	8622	8576
R3100F9C	29413	29048	28802	28232	24831	24784

sample-id	input	filtered	denoised	merged	non-chimeric	bact only
R310F1C	47951	47330	46148	42512	30453	30424
R310F2C	29819	29460	28787	26296	17800	#N/A
R310F3C	45244	44675	43695	40633	29411	29406
R310F4C	39842	39348	38639	36007	25145	25108
R310F5C	265	260	249	244	244	244
R310F6C	12866	12705	12193	10919	7816	7808
R310F7C	40334	39869	39240	36578	25497	25414
R310F8C	44285	43770	43368	41973	37471	36956
R310F9C	35287	34839	34101	31433	22655	22649
R31F10C	59346	58502	57188	51853	30988	30776
R31F10xC	1370919	1353110	1344492	1285214	904422	898579
R31F1C	34672	34215	33241	29863	19799	19694
R31F2C	7	7	1	0	0	#N/A
R31F3C	39553	38996	38153	34830	22807	22766
R31F4C	34656	34169	33381	30482	19372	19324
R31F5C	11	11	4	4	4	4
R31F6C	12471	12315	11859	10399	7454	7439
R31F7C	14	14	6	3	3	3
R31F8C	5	5	1	0	0	#N/A
R31F9C	10944	10810	10398	9139	6288	6282
R3CTRLF10C	39469	39014	38215	35391	25109	25016
R3CTRLF1C	31954	31586	30702	27870	18735	18726
R3CTRLF2C	9	9	3	2	2	2
R3CTRLF3C	33344	32868	31920	28533	19179	19006
R3CTRLF4C	12	12	4	2	2	2
R3CTRLF5C	36667	36181	35240	32203	24879	22707
R3CTRLF6C	39882	39396	38400	35026	26088	25950
R3CTRLF7C	40002	39435	38283	34250	23283	23224
R3CTRLF8C	33680	33311	32432	29354	20577	20560
R3CTRLF9C	44403	43843	42560	37778	24163	22309
NTC2D	593	583	526	429	384	378
NTCD	8	8	2	2	2	2

79 **Table S3:** Number of nodes and edges from the neighborhood selection networks of the genomic
 80 gut microbiome discovered by rDNA metabarcoding.

Molecule	Exposure ($\mu\text{g g}^{-1}$)	Number of nodes	Number of nodes (non-alone)	Number of edges	cluster-edges
rDNA	0	107	104	131	111
	1	89	73	240	197
	10	90	71	60	57
	100	78	56	44	42
	1000	81	70	75	69

81